Redox-dependent distribution of early macro-organisms: Evidence from the terminal Ediacaran Khatyspyt Formation in Arctic Siberia

Huan Cui [a,b,*], Dmitriy V. Grazhdankin [c,d], Shuhai Xiao [e], Sara Peek [b,1], Vladimir I. Rogov [c], Natalia V. Bykova [e], Natalie E. Sievers [b,2], Xiao-Ming Liu [f], Alan J. Kaufman [b]

[a] Department of Geoscience and NASA Astrobiology Institute, University of Wisconsin–Madison, Madison, WI 53706, USA
[b] Department of Geology and Earth System Science Interdisciplinary Center, University of Maryland, College Park, MD 20742, USA
[c] Trofimuk Institute of Petroleum Geology and Geophysics, Siberian Branch Russian Academy of Sciences, Novosibirsk 630090, Russia
[d] Department of Geology and Geophysics, Novosibirsk State University, Novosibirsk 630090, Russia
[e] Department of Geosciences, Virginia Tech, Blacksburg, VA 24061, USA
[f] Department of Geological Sciences, University of North Carolina, Chapel Hill, NC 27599, USA

ARTICLE INFO

Article history:
Received 30 May 2016
Received in revised form 10 August 2016
Accepted 11 August 2016
Available online 18 August 2016

Keywords:
Chemostratigraphy
Redox condition
Early macro-organism distribution
Carbon and sulfur cycles
Oceanic euxinia
Superheavy pyrite

ABSTRACT

The Ediacaran Period witnessed the first appearance of macroscopic animal life in Earth's history. However, the biogeochemical context for the stratigraphic occurrence of early metazoans is largely uncertain, in part due to the dearth of integrated paleobiological and chemostratigraphic datasets. In this study, a comprehensive geochemical analysis was conducted on the fossiliferous Khatyspyt Formation in Arctic Siberia, in order to gain insights into the Ediacaran paleoenvironments. This study was designed to specifically address the relationship between paleoredox conditions and Ediacaran fossil occurrences in the Khatyspyt Formation. Our data reveal a dramatic shift in pyrite sulfur isotope compositions ($\delta^{34}S_{pyrite}$) from ca. −20‰ to ca. 55‰, and this shift is intriguingly associated with the first occurrence of Ediacara-type macrofossils at the studied section, suggesting a possible link between seawater redox conditions and distribution of early macroscopic organisms. Based on multiple lines of sedimentological and geochemical evidence, we propose that the development of oceanic euxinia — which may be widespread in the continental margins due to enhanced oxidative weathering in the terminal Ediacaran Period — may have locally prohibited the colonization of Ediacara-type organisms and resulted in low $\delta^{34}S_{pyrite}$ values in the lower Khatyspyt Formation. In the middle and upper Khatyspyt Formation, progressive secular transition from euxinic to non-euxinic and more habitable conditions may have allowed for the colonization of Ediacara-type and other macro-organisms.

1. Introduction

The Ediacaran Period (ca. 635–541 Ma) holds the answers to key questions related to the origins of the modern Earth system. In particular, Ediacaran strata contain the planet's first unambiguous evidence of macroscopic metazoans and assemblages of "Ediacara-type" fossils (Xiao and Laflamme, 2009). Our present understanding of the origin of animals depends critically on the ability to interpret fossil impressions in siliciclastic sediments made by the Ediacara-type macro-organisms (Gehling, 1999; Narbonne, 2005; Fedonkin et al., 2007) and to document their spatial and temporal distribution (Grazhdankin, 2011, 2014; Narbonne et al., 2014). However, siliciclastic rocks, particularly coarse-grained sandstones, offer limited opportunities for biogeochemical reconstructions of the deep-time record. Fortunately, Ediacara-type macrofossils can also be preserved in carbonate rocks, including the Khatyspyt Formation in Siberia (Fedonkin, 1990; Nagovitsin et al., 2015; Rogov et al., 2015) and the Dengying Formation in South China (Ding and Chen, 1981; Sun, 1986; Xiao et al., 2005; Chen et al., 2014). Chemostratigraphic investigation of these fossiliferous carbonate successions can provide critical geochemical data that complement our understanding from siliciclastic successions.

Ediacaran animals and perhaps Ediacara-type macro-organisms are believed to be oxygen-breathing life forms (Cloud, 1968; Cloud, 1976; Xiao, 2014), therefore a putative rise in atmospheric oxygen during the Ediacaran Period (Derry et al., 1992; Kaufman et al., 1993) may have dictated their evolutionary trajectories and their environmental distribution. Compilations of redox-sensitive proxies at broad timescale suggest a general pattern of rising atmospheric oxygen levels during the

* Corresponding author at: Department of Geoscience and NASA Astrobiology Institute, University of Wisconsin–Madison, Madison, WI 53706, USA.
E-mail address: Huan.Cui@Wisc.EDU (H. Cui).
[1] Current address: United States Geological Survey, Menlo Park, CA 94025, USA.
[2] Current address: Department of Geological Sciences, School of Earth, Energy & Environmental Sciences, Stanford University, CA 94305, USA.

http://dx.doi.org/10.1016/j.palaeo.2016.08.015

Fig. 1. Map showing measured sections of the Khatyspyt Formation (including the studied 0601 and 0605 sections marked as red dots) along the Khorbusuonka River in the Olenek Uplift, northeastern Siberia, Republic of Sakha, Russia.

late Proterozoic (Kah et al., 2004; Canfield et al., 2007; Kump, 2008; Kah and Bartley, 2011; Shields-Zhou and Och, 2011; Lyons et al., 2014; Planavsky et al., 2014; Liu et al., 2016), although oceanic anoxia has also been argued to remain persistent in many parts of the ocean even in the Ediacaran Period (Canfield et al., 2008; Sperling et al., 2015c; Reinhard et al., 2016; Sahoo et al., 2016). In addition, individual case studies on integrative chemostratigraphy and biostratigraphy of the terminal Ediacaran strata, including the Blueflower Formation in NW Canada (Johnston et al., 2013; Macdonald et al., 2013; Sperling et al., 2015a), the Nama Group in Namibia (Hall et al., 2013; Darroch et al., 2015; Wood et al., 2015), and the Dengying Formation in South China (Duda et al., 2014; Cui et al., 2016a) reveal dynamic redox histories in these depositional basins, suggesting a complex relationship between the emergence of macrometazoans and the putative Ediacaran oxygenation. To further test the various hypotheses about the relationship between the rise of animals and atmospheric oxygen levels, we carried out an integrative investigation of the terminal Ediacaran Khatyspyt Formation in northern Siberia, which contains a moderate diversity of Ediacara-type macrofossils and abundant carbonate rocks for chemostratigraphic analysis (Knoll et al., 1995; Pelechaty et al., 1996a). The goal of this study is to assess the effect of redox conditions on the distribution of early macro-organisms — particularly Ediacara-type macro-organisms — in the Khatyspyt Formation, using carbon, oxygen, sulfur, and strontium isotopes, as well as trace element concentrations.

2. Geological background

2.1. Lithostratigraphy

The fossiliferous Khatyspyt Formation is well exposed along the right-hand side tributaries of the Olenek River (i.e., the Khorbusuonka and Kersyuke rivers) that drains the Olenek Uplift in the northeastern part of the Siberian platform, Republic of Sakha, Russia (Figs. 1 and 2A) (Nagovitsin et al., 2015). Sedimentological observations from the studied Khatyspyt interval (0–130 m in Fig. 3) suggest an overall shelf marine environment with relatively deeper water depth compared with the Maastakh Formation and the overlying Turkut Formation. The lowermost Khatyspyt Formation is dominated by thick packages of intraclastic limestone occurring as channelized bodies up to 7 m in thickness, with abundant tilted angular intraclasts (Fig. 2B) and soft-sediment deformation structures (Fig. 2C), and are laterally persistent over tens to hundreds of meters. The majority of this formation consists of finely laminated medium-bedded limestone with occasional small cross beddings (Fig. 2D). The succession also includes intervals of alternating thin layers of limestone and shale (Fig. 2E), abundant carbonaceous compressions preserved on the bedding planes (Fig. 2F), packages of thin-bedded (Fig. 2G) and thick-bedded limestone (Fig. 2H). The latter often show wavy bedding (Fig. 2J). Finely laminated limestones (Fig. 2I) sometimes contain dense assemblage of *Nenoxites* fossils, which were initially regarded as meniscate trace fossils

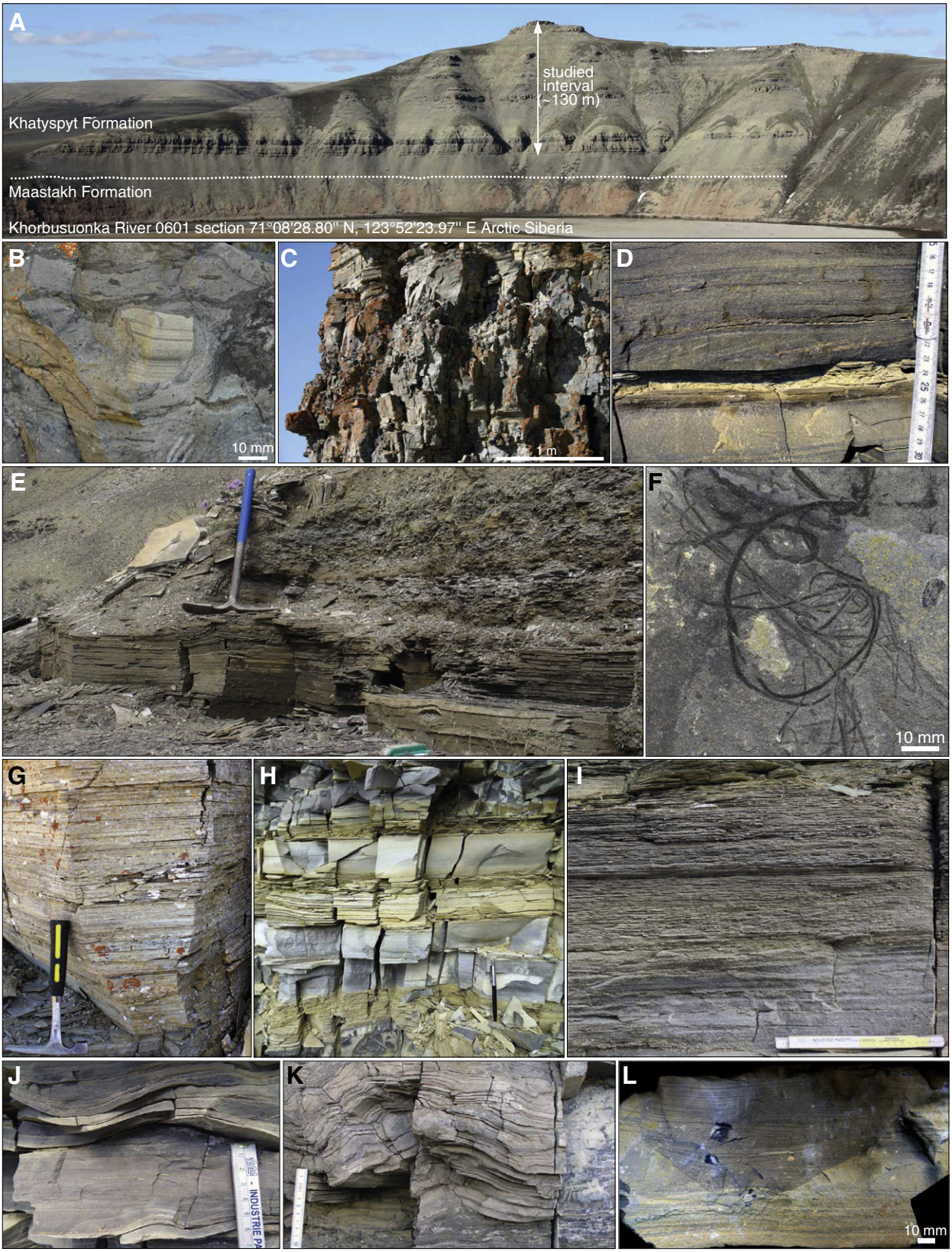

Fig. 2. Sedimentary features of the Khatyspyt Formation. (**A**) Outcrop of the Khatyspyt Formation and stratigraphic position of the studied interval; (B) Intraclastic limestone suggesting a local slope break in a ramp setting; (C) Dolomitized intraclastic limestones with soft-sediment deformation structures suggesting a local slope break in a ramp setting; (D) Cross-bedded limestone in a mid-ramp setting; (E) Alternating limestones and shales in an outer ramp setting; (F) Carbonaceous compressions preserved on a bedding plane of finely laminated limestones; (G) Thin-bedded limestones in a mid-ramp setting; (H) Alternating thin-bedded and thick-bedded limestone characteristic of a distal mid ramp to proximal outer ramp zone (pencil for scale); (I) Thin-bedded limestone with debated ichnofabric in an outer to mid-ramp setting; (J) Wavy-bedded limestone in a mid-ramp setting; (K) Soft-sediment deformation structures in the interval of limestone-shale alternations suggesting a local slope break in a ramp setting; (L) Thin-bedded limestone gutter cast in an inner ramp setting. The scales in I, J and K are around 21 cm, 7 cm, and 10 cm in length, respectively. Please refer to Fig. 3 for stratigraphic position of each photograph.

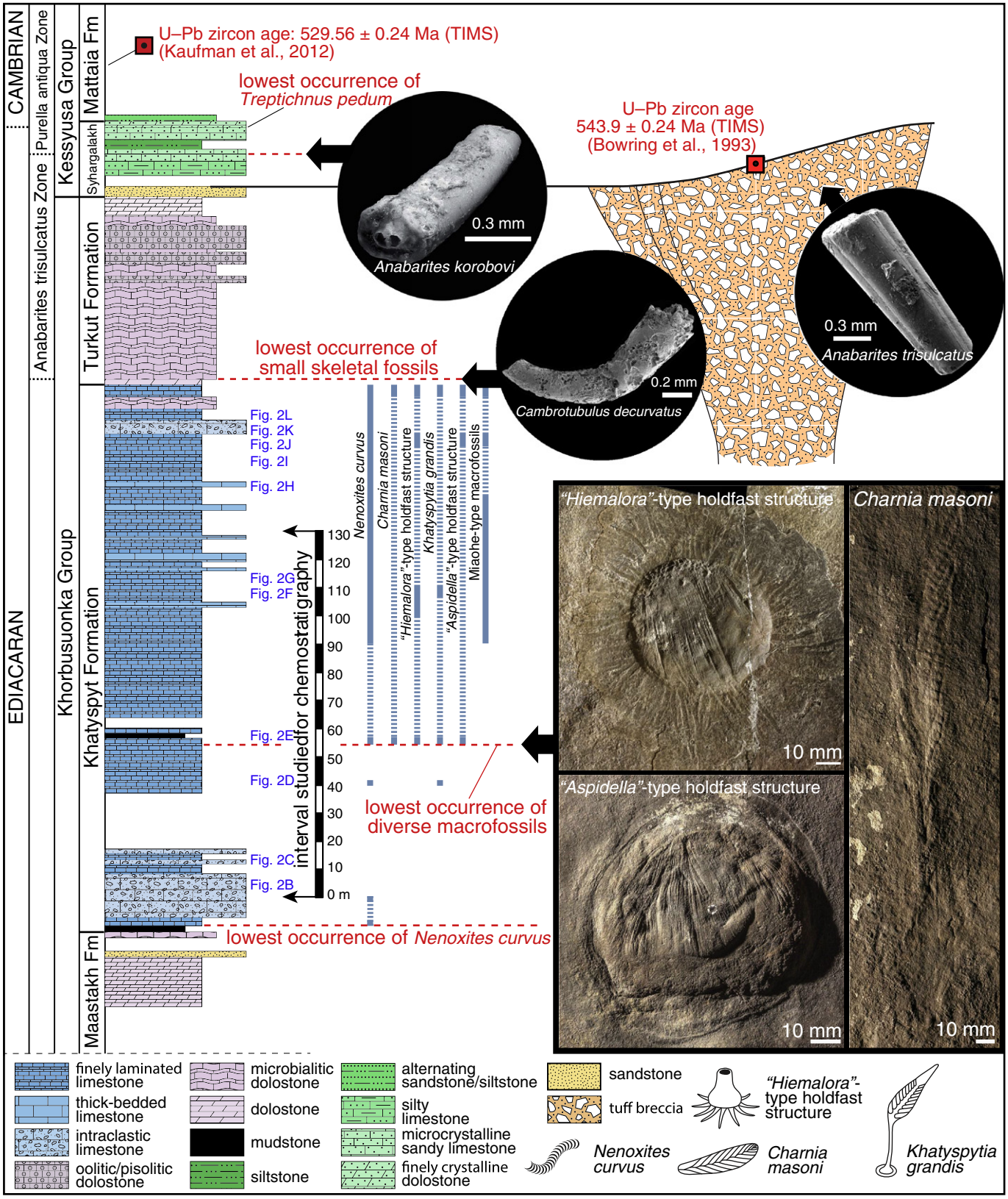

Fig. 3. Integrated litho-, bio- and chrono-stratigraphy of the Khorbusuonka and lowermost Kessyusa groups in Arctic Siberia. Controversial *Nenoxites/Shaanxilithes*-type structure occurs in the basal Khatyspyt Formation, which may represent the oldest evidence of bioturbation (Rogov et al., 2012), or enigmatic ribbon-shaped body fossils (Shen et al., 2007; Meyer et al., 2012; Tarhan et al., 2014). Typical Ediacara-type fossils were found in the middle Khatyspyt Formation (Grazhdankin et al., 2008). Small skeletal fossils were found in the overlying Turkut and Syhargalakh formations (Nagovitsin et al., 2015). The Turkut Formation is penetrated by diatremes that yielded a U–Pb zircon date of 543.9 ± 0.3 Ma (Bowring et al., 1993). The small shelly fossil *Anabarites trisulcatus* was found in limestone clasts in the tuff breccia from the diatreme. The limestone clasts are inferred to have derived from the Turkut Formation, although the exact stratigraphic horizon of *Anabarites trisulcatus* has not yet been located in the Turkut Formation. A new U–Pb zircon date of 529.56 ± 0.24 Ma has recently been reported for a volcanic tuff in the Mattaia Formation (Kessyusa Group) higher in the sequence (Kaufman et al., 2012). Both ages are measured by TIMS (Thermal Ionization Mass Spectrometer).

(Sokolov and Fedonkin, 1984; Rogov et al., 2012, 2013a, 2013b, 2015), but have alternatively been interpreted as enigmatic tubular body fossils similar to *Shaanxilithes* that has been reported from the terminal Ediacaran strata in South China and India (Hua et al., 2004; Shen et al., 2007; Meyer et al., 2012; Brasier et al., 2013; Gámez Vintaned and Zhuravlev, 2013; Mángano and Buatois, 2014; Tarhan et al., 2014). The uppermost Khatyspyt Formation is characterized by soft-sediment slump and deformation features (Fig. 2K) and gutter cast structures (Fig. 2L). Sedimentological observations suggest deposition within a starved intracratonic rift developed in a marine ramp setting, with intraclastic limestone representing debris flows deposited adjacent to inferred syn-sedimentary faults (Knoll et al., 1995; Pelechaty et al., 1996a; Nagovitsin et al., 2015).

The Khatyspyt Formation overlies pebble-bearing trough and tabular cross-bedded channelized sandstone, microbial dolostone and finely laminated shale of the Maastakh Formation, and is overlain by microbial dolostone, cross-bedded oolitic and pisolitic dolostone, microbialite bioherms of the Turkut Formation (Fig. 3). These three formations constitute the Khorbosuonka Group, which is bounded by regional unconformities (Sokolov and Fedonkin, 1984; Knoll et al., 1995; Pelechaty et al., 1996a; Nagovitsin et al., 2015).

2.2. Geochronological constraints

Available geochronometric constraints for the Khorbusuonka Group and the overlying Kessyusa Group are currently based on two ages. A diatreme that penetrates the Turkut and the lowermost Syhargalakh formations in a section along the Khorbusuonka River yield a U–Pb zircon age of 543.9 ± 0.24 Ma (Bowring et al., 1993; Rogov et al., 2015). This age provides a minimum age constraint on the Khatyspyt Formation and a maximum age constraint on the first appearance of the trace fossil *Treptichnus pedum* in the overlying strata of the uppermost Syhargalakh Formation. A U–Pb zircon age of 529.56 ± 0.24 Ma has recently been reported for a volcanic tuff in the Mattaia Formation (Kessyusa Group) higher in the sequence (Kaufman et al., 2012) (Fig. 3). These two ages are consistent with an inferred terminal Ediacaran age for the studied Khatyspyt Formation.

2.3. Biostratigraphy

The Khatyspyt Formation is exceptionally fossiliferous, with multiple taphonomic windows into the Earth's earliest macroscopic communities. The fossil assemblages contain soft-bodied organisms (Avalon-type biota) with moldic preservation through authigenic carbonate cementation, carbonaceous compression macrofossils (Miaohe-type biota) (Grazhdankin et al., 2008; Nagovitsin et al., 2015), and the enigmatic fossil *Nenoxites* (Rogov et al., 2012). The fossils are unevenly distributed in the Khatyspyt Formation. Apart from sporadic occurrences of *Nenoxites*, rare low-relief discoidal structures (microbial colonies sensu Grazhdankin and Gerdes, 2007), and a single small individual resembling *Khatyspytia grandis*, the lower part of the formation (i.e., the interval of 0–67.7 m from the base) is essentially unfossiliferous. The interval from 15 m to 40 m was not sampled because of poor exposure, resulting in an incomplete lithostratigraphic column of the lower Khatyspyt Formation. Regardless, field inspection of available outcrops in this interval suggests that it is non-fossiliferous, although future investigation of better exposures is needed to verify this observation.

Diverse Avalon-type fossils, including the globally distributed rangeomorph taxon *Charnia masoni*, "*Hiemalora*"-type holdfast structures (sensu Hofmann et al., 2008), and the arboreomorph *Khatyspytia grandis* showing similarities with *Charniodiscus procerus* from Newfoundland (sensu Xiao and Laflamme, 2009), appear suddenly in finely laminated limestones of the Khatyspyt Formation (at ~42 m). There is no visible evidence of any significant change in depositional rate or facies at this stratigraphic level. Avalon-type fossils are found throughout the rest of the Khatyspyt Formation with little variation in taxonomic composition. *Nenoxites* fossils also become increasingly abundant in the upper part of the Khatyspyt Formation. Abundant and diverse carbonaceous compression macrofossils, including some Miaohe-type taxa (Xiao et al., 2002), first appear in the mid-Khatyspyt Formation. The appearance of carbonaceous compressions is not accompanied by notable isotopic perturbation, thus may be related to taphonomic factors (Grazhdankin et al., 2008).

The paleontological characteristics of the Khatyspyt Formation is not particularly indicative of specific Ediacaran stratigraphic age, although macrofossil assemblages consisting of palaeopascichnids, rangeomorph, erniettomorph, and/or arboreomorph frondose taxa in the absence of many other iconic Ediacaran forms usually (but not always) suggest a late Ediacaran age (Kolesnikov et al., 2015; Boag et al., 2016; Darroch et al., 2016). However, it should also be taken with caution that ecological control of Ediacaran organisms may have imposed serious limitation in the use of biostratigraphic correlation (Gehling and Droser, 2013; Grazhdankin, 2004, 2014). Supposing the *Nenoxites* ichnofabric (sensu Rogov et al., 2012) and the body fossil *Shaanxilithes* refer to approximately the same structure, then the latter could be used as a reliable biostratigraphic marker for global correlation of terminal Ediacaran strata immediately preceding the oldest small skeletal fossils (Shen et al., 2007; Zhuravlev et al., 2009; Meyer et al., 2012; Tarhan et al., 2014; Rogov et al., 2015; Darroch et al., 2016; Xiao et al., in press). Indeed, the lowest stratigraphic occurrence of the small skeletal fossil *Cambrotubulus decurvatus* in the northwestern slope of the Olenek Uplift is found to be 1.4 m above the base of the Turkut Formation that conformably overlies the Khatyspyt Formation.

3. Samples and analytical methods

The samples were collected from the Khatyspyt Formation at the 0601 (GPS: 71° 08′ 28.80″ N, 123° 52′ 23.97″ E) and 0605 (GPS: 71° 12′ 17.20″ N, 123° 39′ 35.43″ E) sections. The 0601 section is of particular interest because it has yielded an exceptionally preserved assemblage of diverse Ediacara-type macrofossils, representing the first appearance of these fossils in the Khatyspyt Formation (Fig. 3). Using regionally consistent occurrence of thick-bedded limestones and volcanic tuffs as marker beds, we correlated the 0605 section with a covered interval (90–106 m) at the 0601 section in order to achieve more compete chemostratigraphic sampling (Figs. 4 and 5). The sampled interval in this study covers the lowest occurrence of Ediacara-type macrofossils, and is composed of thin-bedded carbonates deposited in normal marine environments.

A total of 176 samples were systematically analyzed to obtain a complete suite of chemostratigraphic data, including carbonate carbon ($\delta^{13}C_{carb}$) and oxygen isotopes ($\delta^{18}O_{carb}$), strontium isotopes ($^{87}Sr/^{86}Sr$), organic carbon isotopes ($\delta^{13}C_{org}$), sulfur isotopes of total sulfur in acidified residuals ($\delta^{34}S_{TS}$, comprising dominantly pyrite S with trace amount of organic S), carbonate-associated sulfate sulfur isotopes ($\delta^{34}S_{CAS}$), and major and trace element concentrations. Sample preparation work, including sample cutting, crushing, acidification, leaching, and polishing, was conducted at the Trofimuk Institute of Petroleum Geology and Geophysics, Siberian Branch of the Russian Academy of Sciences, Novosibirsk. Elemental analyses were conducted in the Carnegie Institution of Washington. All the isotope analyses were conducted in the Department of Geology, University of Maryland by using standard methods (e.g., McFadden et al., 2008; Cui, 2015; Cao et al., 2016; Cui et al., 2015, 2016a, 2016b, under review), which are briefly outlined below.

3.1. Carbon and oxygen isotope analysis

Rock samples were cut and polished for detailed petrographic observation and micro-drilling in order to obtain powders from the least-altered, least-recrystallized, and purest phases for carbonate carbon and oxygen isotope analysis. The powders were measured with a Multicarb

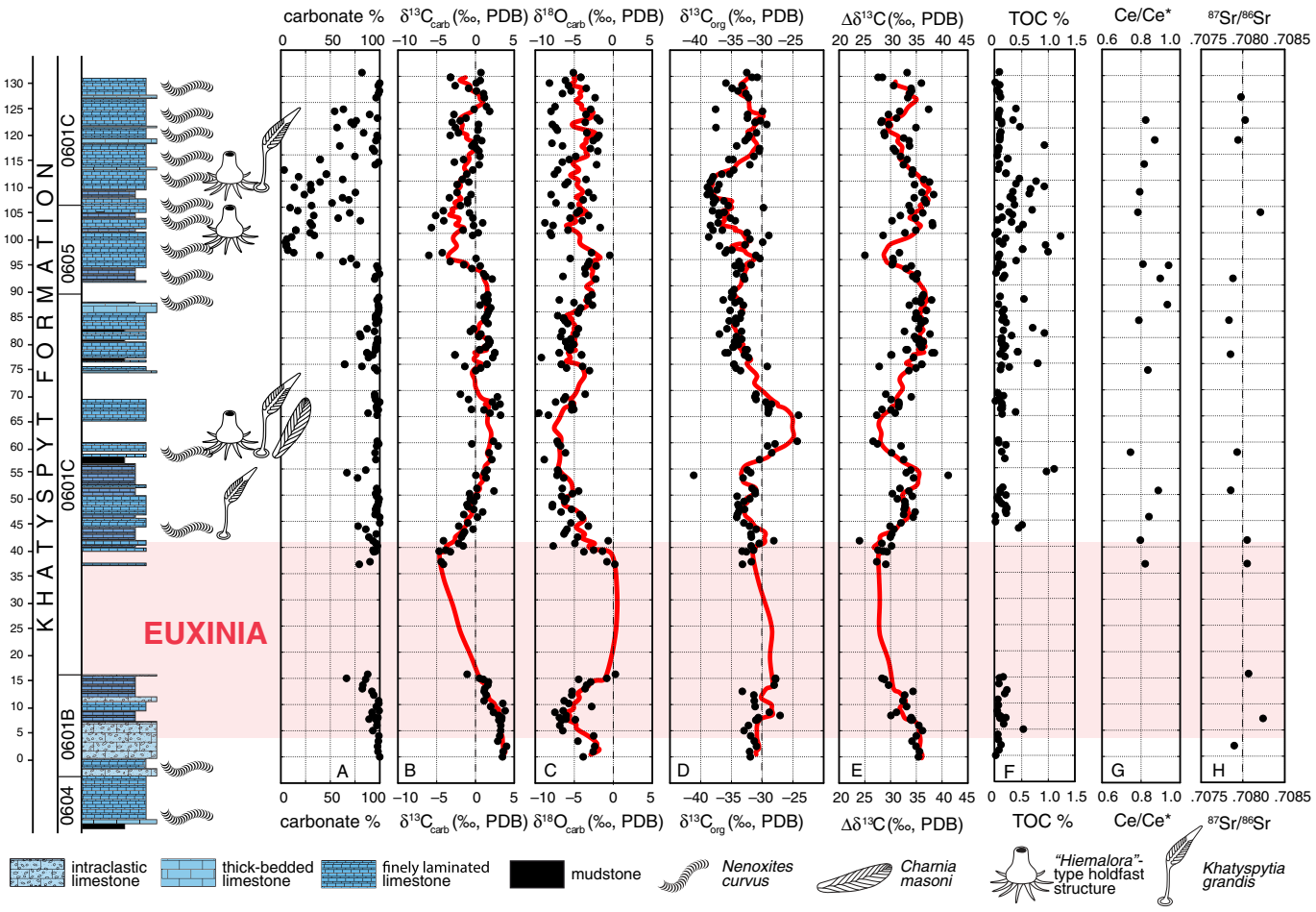

Fig. 4. Chemostratigraphic profiles of the terminal Ediacaran Khatyspyt Formation at the 0601 and 0605 sections, Arctic Siberia. Measured geochemical profiles include carbonate percentage (carbonate%), carbonate carbon ($\delta^{13}C_{carb}$, ‰ V-PDB) and oxygen isotopes ($\delta^{18}O_{carb}$, ‰ V-PDB), organic carbon isotopes ($\delta^{13}C_{org}$, ‰ V-PDB), carbon isotope fractionations ($\Delta\delta^{13}C_{carb\text{-}org}$), total organic carbon content (TOC, %), Ce anomaly (Ce/Ce*) calculated using the formula $Ce/Ce^* = [Ce]_{PAAS} / ([Pr]^2_{PAAS} / [Nd]_{PAAS})$ (Ling et al., 2013), and strontium isotope ratios ($^{87}Sr/^{86}Sr$). The pink background colour represents interpreted euxinic conditions. Red fitted lines represent five-point running average. Poor exposure of the interval from 15 m to 40 m resulted in a sampling gap and an incomplete lithological column in the lower Khatyspyt Formation. Regardless, a limited scope of field observation on available outcrops recovered no fossils in this unsampled interval. No visible change in lithology and facies has been found through this unsampled interval. Refer to Fig. 3 for stratigraphic position of the studied interval.

inlet device in-line with an Elementar Isoprime continuous-flow isotope ratio mass spectrometer, and precision for both isotopes was routinely better than 0.1‰.

3.2. Organic carbon and pyrite sulfur isotope analyses

The organic carbon, total sulfur isotope compositions were measured by combustion of the decalcified residuals to CO_2 or SO_2 with a Eurovector elemental analyzer in-line with a second Elementar Isoprime isotope ratio mass spectrometer. Around 15 g of bulk crushed sample was acidified with 3 M HCl. Acidified residues were washed with ultra-pure Milli-Q (18 MΩ) water, centrifuged, decanted, and dried. The residues were packed into folded tin cups with V_2O_5 for combustion to CO_2 or SO_2 in a Eurovector elemental analyzer in-line with a second Elementar Isoprime isotope ratio mass spectrometer, which measured isotope abundances. Uncertainties for carbon and sulfur isotope measurements determined by multiple analyses of standard materials during analytical sessions are better than 0.1‰ and 0.3‰, respectively.

3.3. Sulfate sulfur isotope analysis

Approximately 100 g of bulk carbonate powders were used for extraction of carbonate-associated sulfate (CAS). To minimize the contamination of soluble non-CAS sulfate (Marenco et al., 2008; Wotte et al., 2012; Peng et al., 2014; Schobben et al., 2015), bulk powders were leached by 10% NaCl until no sulfate could be tested from the leachate, and then washed with Milli-Q water for at least 3 times prior to acidification of the leached powders with 3 M HCl to release CAS. Both non-CAS and CAS precipitates were collected as $BaSO_4$ three days after $BaCl_2$ was added to the solution for $\delta^{34}S_{leachate}$ and $\delta^{34}S_{CAS}$ analyses, respectively. The $BaSO_4$ precipitates were packed into folded tin cups with V_2O_5 for combustion to SO_2 in a Eurovector elemental analyzer in-line with a second Elementar Isoprime isotope ratio mass spectrometer. Uncertainties for sulfur isotope measurements determined by multiple analyses of standard materials during analytical sessions are better than 0.3‰. Sulfur isotope fractionation between sulfide and sulfate are calculated as $\Delta\delta^{34}S \approx \delta^{34}S_{CAS} - \delta^{34}S_{TS}$, assuming the sulfur species in the acidified results of our pyrite-rich samples are dominated by pyrite (i.e., $\delta^{34}S_{TS} \approx \delta^{34}S_{pyrite}$).

3.4. Strontium isotope analyses

For strontium isotope analysis, only limestone samples were selected for extraction and measurement. Micro-drilled powders (ca. 10 mg) were leached three times in 0.2 M ammonium acetate (pH ~ 8.2) to remove exchangeable Sr from non-carbonate minerals, and then rinsed three times with Milli-Q water. The leached powder was centrifuged,

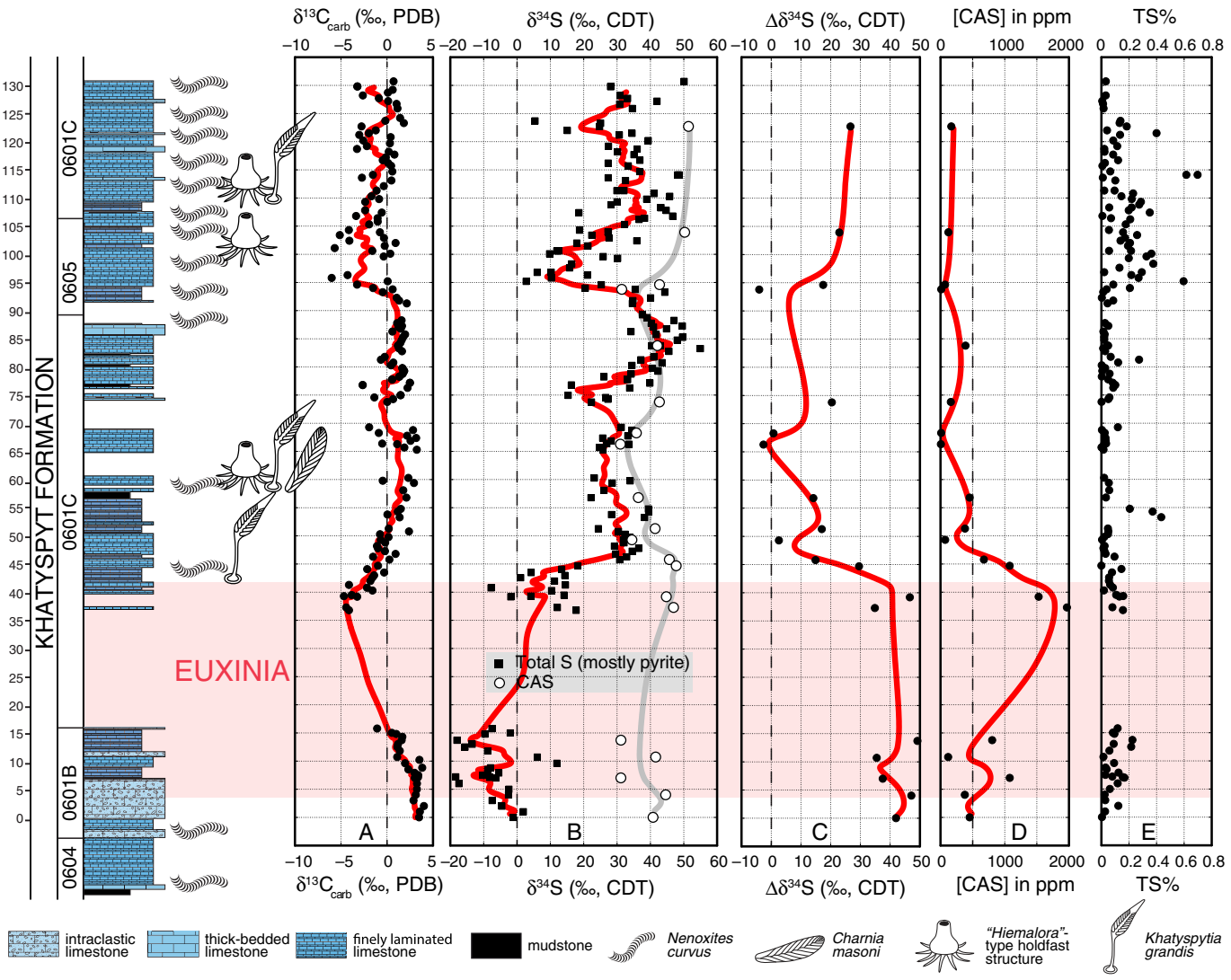

Fig. 5. Chemostratigraphic profiles of the terminal Ediacaran Khatyspyt Formation at the 0601 and 0605 sections, Arctic Siberia. Measured geochemical profiles include carbonate carbon isotopes ($\delta^{13}C_{carb}$, ‰ V-PDB), total sulfur isotopes in acified residuals ($\delta^{34}S_{TS}$, ‰ V-CDT; including pyrite and trace amount of organic S), carboante-associated sulfate sulfur isotopes ($\delta^{34}S_{CAS}$, ‰ V-CDT), sulfur isotope fracionations ($\Delta\delta^{34}S_{CAS\text{-}pyrite}$) assuming the $\delta^{34}S_{TS}$ signals are dominantly derived from pyrite, total sulfur content (TS%, dominated by pyrite with trace amount of organic S), and carbonate-associated sulfate concentration ([CAS] in ppm). The pink background colour represents euxinic conditions. Fitted lines represent five-point running average for $\delta^{13}C_{carb}$ and $\delta^{34}S_{TS}$ data, and two-point running average for $\delta^{34}S_{CAS}$, $\Delta\delta^{34}S$ and [CAS] data. Poor exposure of the interval from 15 m to 40 m resulted in a sampling gap and an incomplete lithological column in the lower Khatyspyt Formation. Regardless, a limited scope of field observation on available outcrops recovered no fossils in this unsampled interval. No visible change in lithology and facies has been found through this unsampled interval. Please refer to Fig. 3 for stratigraphic position of the studied interval.

decanted, and acidified with doubly distilled 0.5 M acetic acid overnight to release strontium from the carbonate crystal structure. The supernatant was centrifuged to remove insoluble residues and then decanted, dried, and subsequently dissolved in 200 μl of 3 M HNO_3. Strontium separation was carried out via cation exchange using a small polyethylene column containing ~1 cm of Eichrom Sr specific resin. The column was rinsed with 400 μl of 3 M HNO_3 before the dissolved sample was loaded onto the column. After loading, the sample was sequentially eluted with 200 μl of 3 M HNO_3, 600 μl of 7 M HNO_3, and 100 μl of 3 M HNO_3 to remove the Ca, Rb and REE fractions; the Sr fraction adsorbs strongly to the resin in an acidic environment. The Sr fraction was removed by elution with ~800 μl of 0.05 M HNO_3 and the resultant eluate collected and dried. Approximately 200–300 ng of the dried sample was transferred onto a degassed and pre-baked (~4.2 A under high vacuum) high purity Re filament with 0.7 μl of Ta_2O_5 activator. The prepared filaments were measured using the VG Sector 54 thermal ionization mass spectrometer (TIMS) facility in the University of Maryland Geochemistry Laboratories. Filaments were transferred to a sample carousel, heated under vacuum ($\sim 10^{-7}$ to 10^{-8} atm) to a temperature between 1450 °C and 1650 °C, and analyzed when a stable signal (>1.0 V) was detected on the mass 88 ion beam. Approximately 100 $^{87}Sr/^{86}Sr$ ratios were collected for each sample. Final data have been corrected for fractionation using the standard value $^{87}Sr/^{86}Sr = 0.1194$. The fraction of ^{87}Sr resulting from in situ decay from ^{87}Rb was removed by measurement of rubidium abundance at mass 85. Repeated analysis of the NBS SRM987 standard yields an average value of $^{87}Sr/^{86}Sr = 0.710245 \pm 0.000011$ (2σ) during the analytical window.

3.5. Elemental analyses

Based on petrographic observations, carbonate samples with low detritus contents were selected for major and trace element analysis. Aliquots of micro-drilled carbonate powders were dissolved in 0.4 M HNO_3, centrifuged, and then analyzed for elemental concentrations. The resulting solutions were analyzed on a Thermo Scientific iCAP-Q ICP-MS (Inductively Coupled Plasma – Mass Spectrometry) at the

Carnegie Institution of Washington. Precision of these analyses as determined by repeated measurements of a house standard carbonate was <5% (2σ) for major elements with high concentrations and <10% (2σ) for the REEs. Cerium anomaly values are calculated by using the formula $Ce/Ce^* = [Ce]_{PAAS} / ([Pr]^2_{PAAS} / [Nd]_{PAAS})$ in order to further constrain the redox conditions of the depositional environment (e.g., Lawrence et al., 2006; Ling et al., 2013; Cui et al., 2015, 2016a).

4. Geochemical results

4.1. $\delta^{13}C_{carb}$ and $\delta^{18}O_{carb}$ data

Chemostratigraphic profiles of the Khatyspyt Formation reveal strong fluctuations in carbon and sulfur isotope compositions (Figs. 4 and 5). The percent carbonate values of most limestone samples are high (approaching 100%) except the shaly interval in the 0605 section (Fig. 4A). Carbonate carbon isotope ($\delta^{13}C_{carb}$) data show a positive excursion (up to ca. 5‰) in the intraclastic limestone interval of the 0601B section, and then decrease to lower values (Fig. 4B). The lower 45 m of the measured section generally reveals a $\delta^{13}C_{carb}$ negative excursion and is succeeded by more positive values up section. Carbonate oxygen isotopes ($\delta^{18}O_{carb}$) mostly remain −5‰, except a slight positive excursion to ca. 0‰ in the lower 45 m (Fig. 4C).

4.2. $\delta^{13}C_{org}$ and TOC data

Total organic carbon content data in the Khatyspyt Formation (Fig. 4F) are generally high (0.28% ± 0.4, 1σ) compared with time-equivalent Gaojiashan Member in South China (0.08% ± 0.15, 1σ). Organic carbon isotope values ($\delta^{13}C_{org}$) are mostly between −30‰ and −40‰ (Fig. 4D), providing a relatively large total carbon isotope fractionation ($\Delta\delta^{13}C$) (Fig. 4E) compared with some older Ediacaran successions (McFadden et al., 2008; Sansjofre et al., 2011; Cui et al., 2015) or the Phanerozoic record (Hayes et al., 1999; Oehlert et al., 2012; Oehlert and Swart, 2014).

4.3. $\delta^{34}S_{py}$ and $\delta^{34}S_{CAS}$ data

A dramatic increase in pyrite sulfur isotopic compositions ($\delta^{34}S_{pyrite}$) from ca. –20‰ to as high as ca. +55‰ occurs in the lower Khatyspyt Formation in the 0601 section (Fig. 5B). Such a large magnitude of $\delta^{34}S_{pyrite}$ excursion has never been reported in the terminal Ediacaran Period (see equivalent chemostratigraphic records in Fike and Grotzinger, 2008; Ries et al., 2009; Cui et al., 2016a) (Fig. 7). Two stages could be defined to describe this dramatic $\delta^{34}S_{pyrite}$ excursion. The lower 45 m (Stage 1), sampled at section 0601B and lower part of section 0601C, is characterized by negative $\delta^{34}S_{pyrite}$ values and an increase from −20‰ to ca. 0‰. The next 85 m of the measured Khatyspyt Formation (Stage 2) is characterized by positive $\delta^{34}S_{pyrite}$ values with an average value of 31.7‰ ± 10.1‰ (1σ) and maximum value as high as +55‰. In contrast with this dramatic variation in $\delta^{34}S_{pyrite}$, sulfur isotope values ($\delta^{34}S_{CAS}$) of carbonate-associated sulfate (CAS) are less variable, with an average value of +40.7‰ ± 6.5‰ (1σ). Assuming the sulfur species in the acidified residuals of our samples are dominated by pyrite (e.g., McFadden et al., 2008; Zhelezinskaia et al., 2014; Cui et al., 2016a), calculated sulfur isotope differences ($\Delta\delta^{34}S$) between sulfate and pyrite are large in the lower 45 m (up to 50‰), but decline to lower and even negative values up section (Fig. 5C). Coincident with the large positive excursion in $\delta^{34}S_{pyrite}$ is a dramatic decrease in CAS concentration (Fig. 5D). CAS concentration data in the lower 50 m are remarkably high (up to almost 2000 ppm), but drop to much lower values (ca. 100 ppm) in the upper section. Total sulfur concentration (TS) data are generally below 0.2%, with higher values in the shaley interval of the 0605 section (Fig. 5E). Intriguingly, the first appearance datum (FAD) of soft-bodied Ediacara-type macro-organisms coincides with the negative-to-positive shifts in both $\delta^{13}C_{carb}$ and $\delta^{34}S_{pyrite}$ in the lower Khatyspyt Formation (Figs. 4 and 5).

4.4. $^{87}Sr/^{86}Sr$ and elemental concentration data

$^{87}Sr/^{86}Sr$ values in the Khatyspyt Formation (Fig. 4H) are ca. 0.7080 ± 0.0001 (1σ), which are consistent with published data from the same section (Vishnevskaya et al., 2013). Rb/Sr and Mn/Fe concentration ratios of the samples analyzed for $^{87}Sr/^{86}Sr$ are all consistently low, which are mostly <0.01 and <0.1, respectively. Ce/Ce* data (Fig. 4G) remain steady values of 0.84 ± 0.06 (1σ) throughout the section.

5. Discussion

5.1. Diagenetic evaluation

Multiple lines of evidence (Fig. 6) suggest that the measured samples from the Khatyspyt Formation are well preserved, and experienced little diagenetic alteration. In contrast with the proposed diagenetic alteration trend (Arthur, 2009; Knauth and Kennedy, 2009; Derry, 2010; Oehlert and Swart, 2014), which typically shows a positive correlation between $\delta^{13}C_{carb}$ and $\delta^{18}O_{carb}$ resulting from meteoric water alteration and organic carbon oxidation during fluid percolation, the Khatyspyt samples shows a broadly negative correlation between $\delta^{13}C_{carb}$ and $\delta^{18}O_{carb}$ (Fig. 6A), suggesting little influence by meteoric water or deep burial.

It has been proposed that sulfur isotopic compositions of carbonate-associated sulfate ($\delta^{34}S_{CAS}$) could possibly be contaminated by pyrite oxidation (Marenco et al., 2008; Wotte et al., 2012; Theiling and Coleman, 2015) or secondary atmospheric sulfate (Peng et al., 2014). If true, cross plot between CAS content and $\delta^{34}S_{CAS}$ should follow a mixing line. However, [CAS]–$\delta^{34}S_{CAS}$ cross plot reveal little correlation (Fig. 6F), suggesting minimum contamination in the measured $\delta^{34}S_{CAS}$ values. Another line of evidence supporting the fidelity of our $\delta^{34}S_{CAS}$ data comes from the general consistency with comparable $\delta^{34}S$ values (ca. 40‰) of bedded anhydrite from the terminal Ediacaran Ara Group in Oman (Fike and Grotzinger, 2008, 2010), suggesting a global seawater signal of ca. 40‰. The consistent $\delta^{34}S_{CAS}$ values (ca. 40‰) independent of [CAS] abundances in the Khatyspyt Formation are also consistent with previous studies (Lyons et al., 2004; Gill et al., 2008; Cui et al., 2016a), demonstrating that CAS can track seawater sulfate compositions. We also plot concentration data against isotopic data (e.g., $\delta^{13}C_{org}$–TOC, $\delta^{34}S_{TS}$–TS) in order to test whether any diagenetic processes could preferentially change the isotopic compositions. These cross-plots show little correlation (Fig. 6B, C) as would be expected from diagenetic alteration.

In addition to $\delta^{34}S_{TS}$ and $\delta^{34}S_{CAS}$ data, sulfur isotope compositions of non-CAS from leachate solutions ($\delta^{34}S_{leachate}$) were also analyzed (Fig. 6G). The $\delta^{34}S_{leachate}$ data are mostly higher than $\delta^{34}S_{TS}$ in the lower 45 m of the section. In contrast, $\delta^{34}S_{leachate}$ values are mostly lower than the $\delta^{34}S_{TS}$ in the upper Khatyspyt Formation where superheavy pyrite is common. The sources of sulfate in the leachate solution could be diverse, including pyrite oxidation (Marenco et al., 2008; Wotte et al., 2012; Theiling and Coleman, 2015), secondary atmospheric sulfate (Peng et al., 2014), or loosely bounded secondary sulfate derived from diagenetic fluids. Thus, $\delta^{34}S_{leachate}$ values may be controlled by various geological factors at different stratigraphic intervals. Regardless, it is notable that all $\delta^{34}S_{CAS}$ data are consistently higher than $\delta^{34}S_{leachate}$ data, demonstrating the importance of leaching pretreatment before CAS extraction.

In summary, sedimentological observations and geochemical data suggest that the limestones in the studied Khatyspyt Formation are well preserved, and provide reliable geochemical signals for chemostratigraphic interpretation.

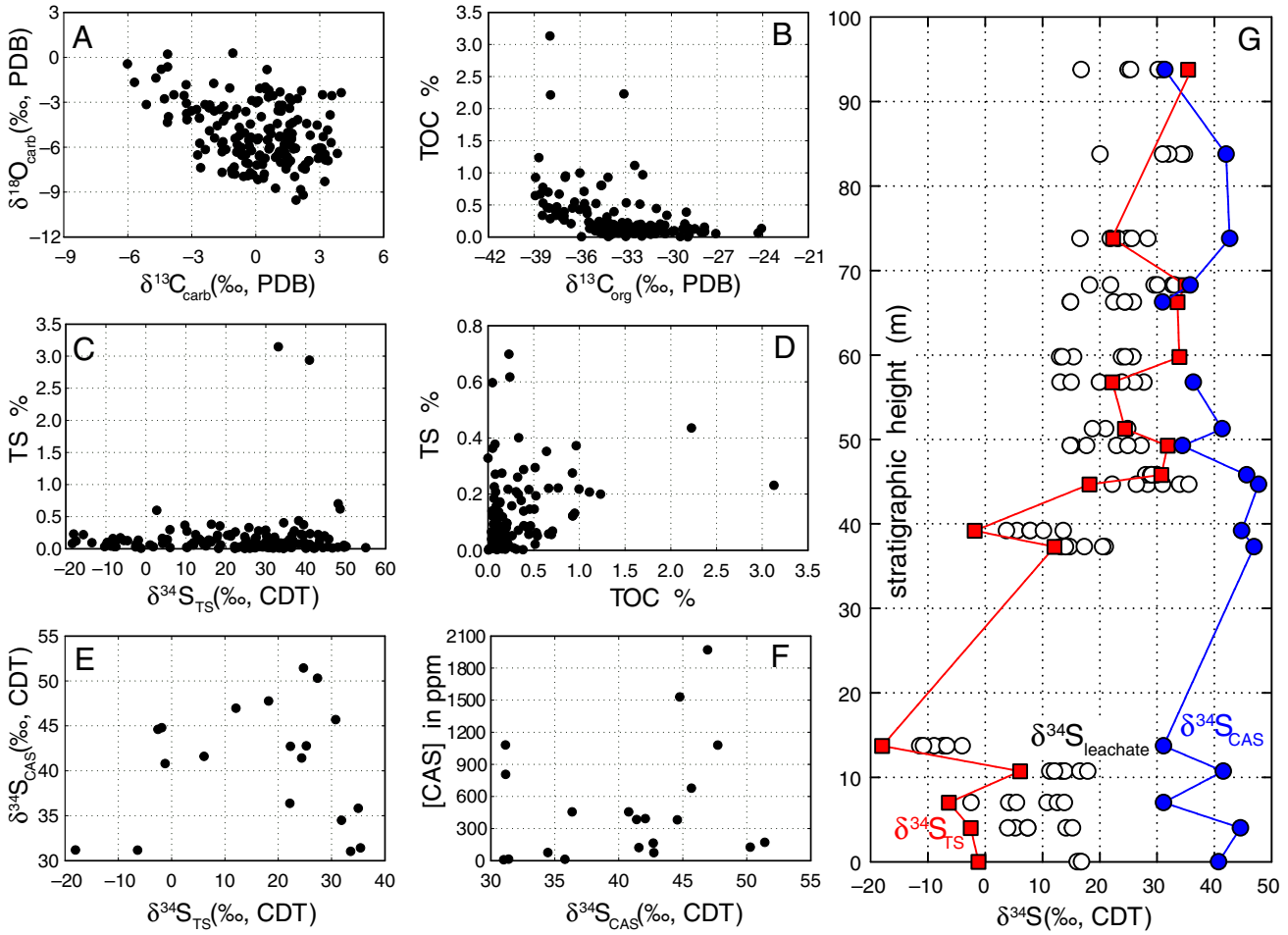

Fig. 6. (A–F) Cross plots of $\delta^{13}C_{carb}$–$\delta^{18}O_{carb}$, $\delta^{13}C_{org}$–TOC%, $\delta^{34}S_{TS}$–TS%, TOC%–TS%, $\delta^{34}S_{TS}$– $\delta^{34}S_{CAS}$, $\delta^{34}S_{CAS}$–[CAS]. (G) Sulfur isotope data of total sulfur ($\delta^{34}S_{TS}$, red), carbonate-associated sulfate ($\delta^{34}S_{CAS}$, blue), and leachate solutions ($\delta^{34}S_{leachate}$, empty circles) collected during leaching. Note that the $\delta^{34}S_{leachate}$ data are systematically higher than $\delta^{34}S_{TS}$ in the lower 45 m, while are generally lower than the $\delta^{34}S_{TS}$ data measured from acidified residuals dominated by superheavy pyrite in the upper section. All $\delta^{34}S_{CAS}$ data are higher than $\delta^{34}S_{leachate}$ data, demonstrating the significance of leaching pretreatment before CAS extraction. All the data are measured from the studied interval in the Khatyspyt Formation at the 0601 and 0605 sections, Arctic Siberia.

5.2. Redox constraints for the depositional basin

The dominance of carbonate lithology and the presence of Ediacaran-type fossils in the Khatyspyt Formation provide important geobiological links between early macro-organisms and their marine environments (Xiao et al., 2013). However, because the most widely used tools for redox reconstruction of marine sediments—including iron speciation analysis (e.g., Canfield et al., 2007, 2008; Poulton and Canfield, 2011) and redox-sensitive trace element analysis (e.g., Scott et al., 2008; Sahoo et al., 2012, 2016; Li et al., 2015b)—are best calibrated for shale lithofacies (but see also Clarkson et al., 2014; Wood et al., 2015), constraints on the redox conditions of the Khatyspyt Formation need to be sought elsewhere.

Given the intimate link between cerium abundance in carbonates and seawater/porewater redox conditions (e.g., Zhou et al., 2012; Ling et al., 2013), cerium anomaly $Ce/Ce^* = [Ce]_{PAAS} / ([Pr]^2_{PAAS} / [Nd]_{PAAS})$ has been explored to constrain the redox conditions of the depositional environment. Cerium exists in two redox states in marine environments, namely Ce(III) and Ce(IV). Trivalent Ce can be oxidized into tetravalent Ce in oxic environments (Tanaka et al., 2010), and then scavenged by Mn-oxides and hydroxides and removed from the seawater. Thus, in oxygenated seawaters, tetravalent Ce is preferentially removed from the system, leaving the seawaters with a Ce negative anomaly in REE patterns. In contrast, trivalent Ce is more soluble in reduced environments, resulting in relatively high Ce/Ce* values (Bau et al., 1996). Therefore, Ce/Ce* ratios of carbonates may help to trace redox changes in seawater/porewater if the samples have not yet experienced significant diagenetic alteration. Here in the Khatyspyt Formation, Ce/Ce* values of well-preserved limestone samples are consistently high throughout the section, with an average value of 0.84 ± 0.06 (1σ), suggesting possible anoxic conditions.

Supporting evidence for an overall anoxic condition of the Khatyspyt Formation also comes from sedimentological observations in the field, where limestones are mostly finely laminated and remarkably rich in organic matter, including bitumen. Total organic carbon (TOC) abundances in most of the carbonate samples are high (0.28% in average) compared with the correlative Gaojiashan Member (0.08% in average), and $\delta^{13}C_{org}$ values range from −24.1‰ to −38.9‰ and average at −33.2‰, suggesting the possible presence of chemoautotrophic or methanotrophic communities at the oxic-anoxic interface in the water column or sediments (Hayes, 1993; Brocks et al., 2005; Johnston et al., 2009; Jiang et al., 2012; Houghton et al., 2014; Guo et al., 2015).

Sulfur isotope data and sulfur abundance data have also been used to constrain the redox conditions of the Khatyspyt Formation. In the lower 45 m of the studied interval, negative $\delta^{34}S_{pyrite}$ values (as low as −20‰) and remarkably high sulfate contents ([CAS] up to 1969 ppm) suggest strong euxinic conditions and syngenetic pyrite formation in the water column (e.g., Canfield and Teske, 1996; Li et al., 2010; Cui et al., 2016a; Kah et al., 2016); whereas in the upper 85 m of the measured section, relatively lower [CAS] concentrations and anomalously high $\delta^{34}S_{pyrite}$ values suggest non-euxinic conditions in the water column

and authigenic pyrite precipitation within marine sediments in an environment with relatively low sulfate concentration (e.g., Ries et al., 2009; Fike et al., 2015; Wu et al., 2016), although the marine sulfate reservoir was large enough to be isotopically buffered, as suggested by the relatively invariant $\delta^{34}S_{CAS}$ values.

Collectively, integrated sedimentological and geochemical data suggest that the Khatyspyt Formation records a transition from euxnic conditions in the lower 45 m to non-euxinic conditions in the upper 85 m.

5.3. Stratigraphic correlation at a global scale

In order to investigate the effect of redox conditions on early metazoans at a global scale, four upper Ediacaran successions are considered for integrated stratigraphic correlation: the Ara Group in Oman, the Nama Group in Namibia, the Gaojiashan/Shibantan Member in South China, and the Khatyspyt Formation in Arctic Siberia (Fig. 7). The late Ediacaran age of these sections is supported by biostratigraphic data and corroborated by available U–Pb zircon dates from volcanic tuffs (Bowring et al., 1993; Grotzinger et al., 1995; Amthor et al., 2003; Condon et al., 2005; Halverson, 2006). Chemostratigraphic data in high stratigraphic resolution are all available for these four successions (Fike and Grotzinger, 2008; Ries et al., 2009; Cui et al., 2016a).

5.3.1. Chemostratigraphic $\delta^{13}C$ correlation

Integrated sedimentological, stratigraphic, and geochemical studies of carbonate successions of terminal Ediacaran records demonstrate the utility of carbon isotope chemostratigraphy for intra- and inter-basinal correlations. The late Ediacaran $\delta^{13}C_{carb}$ record of northeastern Siberia reflects global variations seen elsewhere, featuring (in ascending order) a strong $\delta^{13}C_{carb}$ positive shift to values near 6‰ in the Maastakh Formation and basal Khatyspyt Formation, an intermediate interval of relatively little isotopic change with a monotonic decrease in $\delta^{13}C_{carb}$ from 2‰ to near 0‰ throughout most of the Khatyspyt Formation and Turkut formations, and a negative excursion to ca. −4‰ just beneath the Ediacaran–Cambrian boundary (Knoll et al., 1995; Pelechaty et al., 1996a, 1996b). Similar $\delta^{13}C_{carb}$ positive excursions have also been revealed in the broadly equivalent Nama Group of southern Namibia (Kaufman et al., 1991; Saylor et al., 1998), the Ara Group in Oman (Fike and Grotzinger, 2008), and the Dengying Formation in South China (Jiang et al., 2007; Zhou and Xiao, 2007; Wang et al., 2014; Cui et al., 2016a).

5.3.2. Chemostratigraphic $^{87}Sr/^{86}Sr$ correlation

Given the much longer residence time of strontium in the ocean than the seawater mixing time, strontium isotopes ($^{87}Sr/^{86}Sr$) have been widely used as a tool for inter-basinal stratigraphic correlation (e.g., Halverson et al., 2007; Cui et al., 2015). Terminal Ediacaran limestones typically have $^{87}Sr/^{86}Sr$ ratios ca. 0.7084, including the fossiliferous Shibantan Member of the Dengying Formation in South China (Jiang et al., 2007), the Blueflower Formation in NW Canada (Narbonne et al., 1994), the Nama and Witvlei groups in Namibia and South Africa (Kaufman et al., 1993), the Tamengo Formation of Corumba Group in Brazil (Gaucher et al., 2003; Boggiani et al., 2010), and the Itapucumi Group in NW Paraguay (Warren et al., 2011). However, $^{87}Sr/^{86}Sr$ values of the Khatyspyt Formation are consistently ca. 0.7080 (Vishnevskaya et al., 2013 and this study), raising questions about a $^{87}Sr/^{86}Sr$ chemostratigraphic correlation between the Khatyspyt Formation and other terminal Ediacaran successions worldwide.

Two possibilities may account for the relatively lower $^{87}Sr/^{86}Sr$ values of the Khatyspyt Formation compared with other roughly equivalent successions mentioned above. Largely due to inappropriate lithology (i.e., dolostone, instead of limestone) in the other sections, the 0.7084 values are mainly based on limited analyses of sections in low stratigraphic resolutions, thus may not represent a complete evolution of the $^{87}Sr/^{86}Sr$ during that time. The overall 0.7080 values of the Khatyspyt Formation thus may reflect primary seawater signals of a time interval that has not yet been captured in other terminal Ediacaran data sets before. Alternatively, it is also possible that the lower $^{87}Sr/^{86}Sr$ values in the Khatyspyt Formation may reflect a secondary signal overprinted by enhanced hydrothermal input (e.g., Frei et al., 2011). We cannot resolve these alternative interpretations with the available data.

5.3.3. Chemostratigraphic $\delta^{34}S$ correlation

Chemostratigraphic profiles of paired sulfur isotopes ($\delta^{34}S_{sulfate}$ and $\delta^{34}S_{py}$) reported from upper Ediacaran Gaojiashan Member in South China (Cui et al., 2016a), Nama Group in Namibia (Ries et al., 2009), and Ara Group in Oman (Fike et al., 2006; Fike and Grotzinger, 2008) reveal both similarities and differences when compared to sulfur isotope profiles of the Khatyspyt Formation (Figs. 7 and 8). All these sections consistently show a large positive shift in $\delta^{34}S_{pyrite}$; however, the absolute values and the magnitude of this positive shift are different among the four successions, which may reflect a global perturbation in S cycling overprinted by local signals (e.g., Loyd et al., 2013; Wood et al., 2015). The sulfate sulfur isotopes are generally steady at around 40‰ in Ara, Gaojiashan, and Khatyspyt units (Fike and Grotzinger, 2010; Cui et al., 2016a). However, the Nama Group shows lower $\delta^{34}S_{CAS}$ values with large variations (27.3‰ ± 10.3‰, 1σ) (Ries et al., 2009). It should be noted that $\delta^{34}S_{sulfate}$ in Oman was measured from bedded anhydrite, while $\delta^{34}S_{sulfate}$ data in the other three successions were measured from extracted carbonate-associated sulfate (CAS). Thus, the $\delta^{34}S_{sulfate}$ profile in Oman is probably more reliable given the possible contamination of CAS during chemical weathering in the field (Peng et al., 2014) or lab extraction (Marenco et al., 2008). Another notable feature is the occurrence of superheavy pyrite ($\delta^{34}S_{pyrite} > \delta^{34}S_{CAS}$) in both Nama Group and the Khatyspyt Formation (Figs. 7 and 8). If we accept the global $\delta^{34}S_{sulfate}$ signal is ca. 40‰ as preserved in evaporates, then the comparatively lower $\delta^{34}S_{CAS}$ values [ca. 27.3‰ ± 10.3‰ (1σ)] in the Nama Group and the anomalously high $\delta^{34}S_{pyrite}$ values in both Nama Group and the Khatyspyt Formation need to be explained (see Section 5.5).

The inconsistent absolute values in sulfur isotopes among different localities may result from potential alteration of $\delta^{34}S_{CAS}$ during post-deposition (e.g., Peng et al., 2014), or locally expressed $\delta^{34}S_{pyrite}$ signals due to largely heterogeneous sulfur reservoirs in the late Ediacaran ocean (cf. Loyd et al., 2012). Nevertheless, the overall increasing trend in $\delta^{34}S_{pyrite}$ and decreasing trend in $\Delta\delta^{34}S$ are consistent among the sections, suggesting an overall redox transition from euxinic conditions to a more ventilated ocean. It should be noted that these euxinic water masses may have largely been constrained within shelf basin environments (Lyons et al., 2014; Cui et al., 2015) instead of an open ocean phenomenon. They may have been synchronized by a global enhancement of sulfate flux into the ocean shelf environment during an oxidation event.

5.4. Controlling factors for the chemostratigraphic $\delta^{34}S$ excursion

Multiple factors, such as the ventilation effect of bioturbation (cf. Canfield and Farquhar, 2009), sealing effect of microbial mat (e.g., Bouougri and Porada, 2007; Cai et al., 2010; Grotzinger and Al-Rawahi, 2014), or change in sedimentation rate (cf. Schiffbauer et al., 2014) of marine sediments, could have potentially caused variation of $\delta^{34}S_{pyrite}$ compositions in the studied Khatyspyt Formation. Here we briefly discuss these factors below.

5.4.1. Ventilation effect of bioturbation

It has been proposed that enhanced ventilation of marine sediments and oxidation of authigenic pyrite could be triggered by bioturbation, which consequently would increase the sulfate concentration in the seawater (Canfield and Farquhar, 2009). The activity of bioturbation is generally low during the late Ediacaran Period (Tarhan and Droser, 2014; Tarhan et al., 2015). Here we tentatively evaluate the intensity of bioturbation via the abundance of the enigmatic *Nenoxites* fossils,

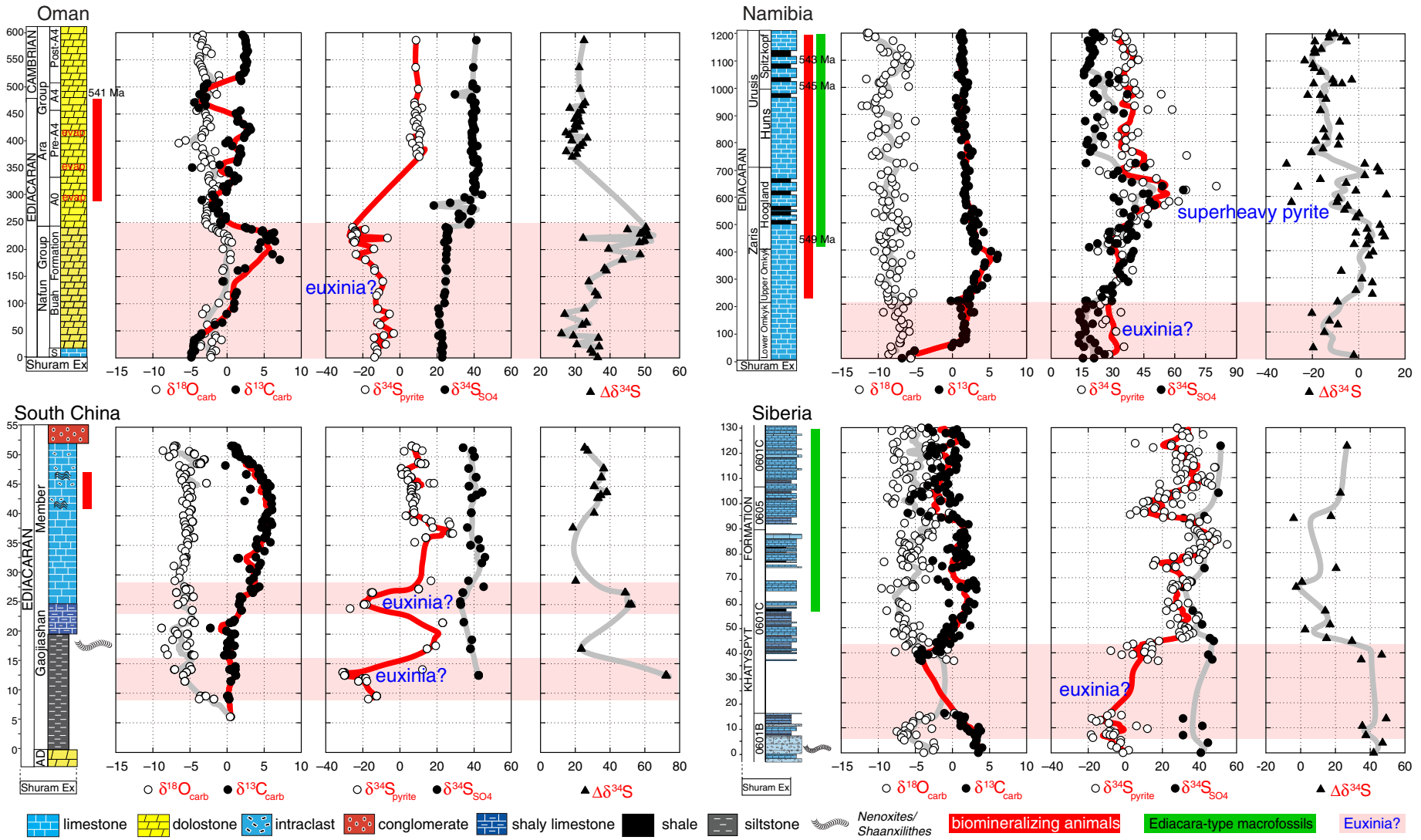

Fig. 7. Global comparison of carbonate C and O isotope data ($\delta^{13}C_{carb}$, $\delta^{18}O_{carb}$), paired S isotope data ($\delta^{34}S_{SO4}$, $\delta^{34}S_{pyrite}$), and sulfur isotope fracionation ($\Delta\delta^{34}S$) data in terminal Ediacaran successions. Data source: Siberia (this study), South China (Cui et al., 2016a), Oman (Fike et al., 2006; Fike and Grotzinger, 2008), and Namibia (Ries et al., 2009). Note that Oman $\delta^{34}S_{SO4}$ data were measured from bedded anhydrite, whereas $\delta^{34}S_{SO4}$ data in Siberia, South China and Namibia were measured from extracted carbonate-associated sulfate (CAS). Fitted lines represent five-point running average for most of the data, and two-point running average for $\delta^{34}S_{CAS}$ and $\Delta\delta^{34}S$ data in Gaojiashan and Siberia due to relatively smaller data set. The pink background colour represents putative euxinic conditions. Biomineralizing animals have been found from sections in Oman (Amthor et al., 2003), Namibia (Germs, 1972) and South China (Bengtson and Zhao, 1992). Frondose Ediacara fossils have been found from sections in Siberia (Grazhdankin et al., 2008) and Namibia (Grotzinger et al., 1995). Similar fossils have also been found in the Shibantan Member in the Yangtze Gorges area (Ding and Chen, 1981; Sun, 1986; Chen et al., 2014), which is generally correlated with the Gaojiashan Member in southern Shaanxi Province of South China. Note that the enigmatic fossil *Nenoxites/Shaanxilithes* also appears to be restricted to non-euxinic intervals in both the Gaojiashan Member (Shen et al., 2007; Meyer et al., 2012) and the Khatyspyt Formation (Rogov et al., 2012).

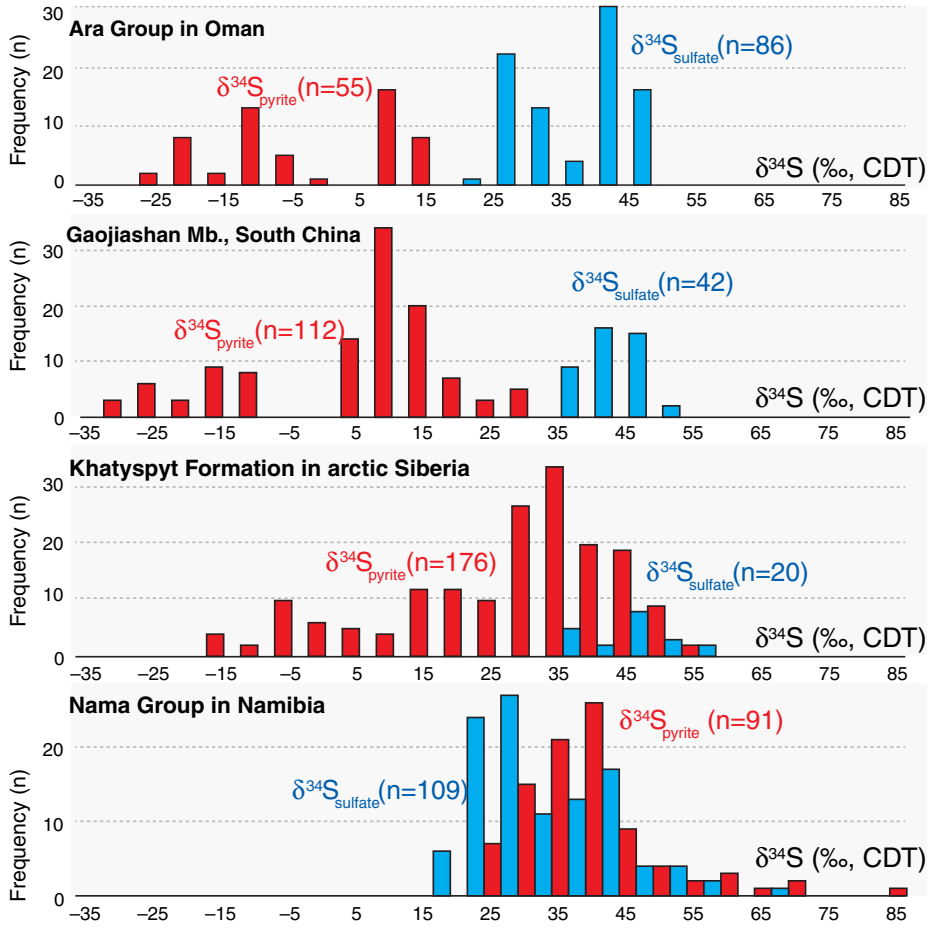

Fig. 8. Histograms showing paired sulfur isotope data ($\delta^{34}S_{pyrite}$ in red, $\delta^{34}S_{sulfate}$ in blue) from the Ara Group in Oman (Fike and Grotzinger, 2008), the Gaojiashan Member in South China (Cui et al., 2016a), the Khatyspyt Formation in Arctic Siberia (this study), and the Nama Group in Namibia (Ries et al., 2009). Note that the $\delta^{34}S_{pyrite}$ data in the Khatyspyt Formation and the Nama Group are anomalously high compared with the other two sections.

though its origin still remains debatable (Brasier et al., 2013; Gámez Vintaned and Zhuravlev, 2013; Mángano and Buatois, 2014; Budd and Jensen, 2015; Rogov et al., 2012, 2013a, 2013b, 2015). If *Nenoxites* fossils indeed result from bioturbation as proposed by Rogov et al. (2012), then it is revealed that bioturbation appears both below and above the euxinic interval, and becomes more abundant starting from ca. 90 m of the studied section (Figs. 4 and 5). However, these intervals with inferred evidence of bioturbation all yield lower [CAS] concentration values (Fig. 5D) instead of higher sulfate concentration predicted by Canfield and Farquhar (2009). Thus, we preclude the possibility of bioturbation as a major controlling factor for the chemostratigraphic $\delta^{34}S$ excursion.

5.4.2. Sealing effect of microbial mat

The occurrence of microbial mats could also potentially influence the $\delta^{34}S$ composition of pyrite in marine sediments. Below non-bioturbated and microbially sealed sediments where the water–sediment interface represents a significant diffusion barrier, pyrite may have higher $\delta^{34}S$ composition. This mechanism may have played a role in the time-equivalent Gaojiashan Member in South China, where chemostratigraphic higher $\delta^{34}S_{pyrite}$ values roughly correspond to the limestone interval with abundant microbial mats (Cui et al., 2016a). However, in the studied Khatyspyt Formation, no clear evidence of microbial mats has been found throughout the section. Thus, this possibility cannot readily explain the observed chemostraitigraphic $\delta^{34}S$ excursion either.

5.4.3. Change in sedimentation rate

Sedimentation rate of marine sediments has been proposed to be a controlling factor in S cycles within the pore water system (Schiffbauer et al., 2014). Higher sedimentation rate may decrease the sulfate diffusion between seawater and pore water, thereby increase the $\delta^{34}S$ composition of authigenic pyrite. However, in the studied Khatyspyt Formation, the lithological facies seem to be largely constant, with no clear depositional change or discontinuity (Figs. 2 and 3). Moreover, negative $\delta^{34}S$ excursion covers both channelized intraclastic limestone (presumably with relatively higher sedimentation rate) and finely laminated limestone (presumably with relatively lower sedimentation rate). Therefore, the scenario of changing sedimentation rate could not readily explain the $\delta^{34}S$ variation in the Khatyspyt Formation.

Taken together, based on the consideration above, it is unlikely that variation in the intensity of bioturbation, abundance of microbial mats, or sedimentation rate could well explain the large $\delta^{34}S$ excursion revealed in this study. In light of similar patterns of $\delta^{34}S$ profiles from roughly equivalent successions in Oman and South China (Fig. 7), it appears that this event is a global phenomenon and directly associated with the formation of distinct superheavy pyrite (see the next section). Thus, the interpretation of the $\delta^{34}S$ profiles should not only explain the

overall positive shift in $\delta^{34}S_{pyrite}$, but also reconcile the remarkably ^{34}S-enriched pyrite in the upper section.

5.5. Biogeochemical origin of the superheavy pyrite

Paired sulfur isotopes of pyrite and sulfate from the Khatyspyt Formation are strongly decoupled. In the measured section, CAS sulfur isotope values are consistently around 40.7‰ ± 6.5‰ (1σ), which are similar to $\delta^{34}S_{CAS}$ data from well-preserved limestone samples in the broadly equivalent Gaojiahsan Member of the Dengying Formation in South China (Cui et al., 2016a) and bedded anhydrite in the Ara Group in Oman (Fike and Grotzinger, 2008) (Figs. 5 and 7). However, sulfur isotope compositions of total sulfur ($\delta^{34}S_{TS}$) in the acidified residuals of the Khatyspyt Formation reveal a large positive shift (Fig. 5B). Assuming sulfur in acidified residuals of these samples is dominantly pyrite (e.g., McFadden et al., 2008; Zhelezinskaia et al., 2014; Cui et al., 2015), calculated sulfur isotope differences between sulfate and sulfide $\Delta\delta^{34}S = \delta^{34}S_{CAS} - \delta^{34}S_{TS}$ are large in the lower Khatyspyt Formation (ca. 40–50‰), transitioning to negative values in the middle section and then to ca. 20–30‰ in the upper section (Fig. 5C). It should be noted, however, that the lack of negative $\Delta\delta^{34}S$ values in the upper Khatyspyt Formation may reflect the limited number of $\delta^{34}S_{CAS}$ analyses. If the global sulfate $\delta^{34}S$ compositions during the terminal Ediacaran Period are 40‰ as recorded in bedded anhydrite in Oman (Fike and Grotzinger, 2008, 2010), a number of samples in the upper 50 m of the Khatyspyt Formation would give negative $\Delta\delta^{34}S$ values.

5.5.1. Published models for superheavy pyrite

Superheavy pyrite and reverse fractionation ($\delta^{34}S_{CAS} < \delta^{34}S_{pyrite}$) have also been reported from the time-equivalent Nama Group in Namibia (Ries et al., 2009) and basal Ediacaran cap carbonates in northwestern China (Shen et al., 2008). Traditional sulfur isotope models have difficulty explaining such phenomenon. Some workers have attributed the reverse fractionation to decoupling of the surface- and bottom-water sulfur reservoirs through ocean stratification (Shen et al., 2008; Kah et al., 2016). This leads to Rayleigh distillation and the formation of ^{34}S-enriched bottom waters, from which sulfate for pyrite precipitation is sourced. Similarly, CAS formed in surface waters could have lower $\delta^{34}S$ values resulting from input from oxidative weathering of terrestrial pyrite (e.g., Shen et al., 2008) or oxidation of deeper euxinic water mass (e.g., Thompson and Kah, 2012; Kah et al., 2016). However, this mechanism would not work in the Khatyspyt Formation, which shows largely invariant $\delta^{34}S_{CAS}$ profile decoupled with the $\delta^{34}S_{pyrite}$ data.

Experimental studies of microbial cultures have shown that the degree of sulfur isotope fractionation accompanying bacterial sulfate reduction (BSR) in seawater approaches to zero when $[SO_4^{2-}]$ is <200 μM (Habicht et al., 2002). This may partly explain the large ^{34}S enrichment of pyrite observed in the Khatyspyt Formation and may reflect low seawater $[SO_4^{2-}]$ in the Proterozoic time. Additionally, the inferred non-euxinic conditions in the upper Khatyspyt Formation means that pyrite formation likely occurred within porewaters, and sulfate availability for BSR may have been limited by diffusion, leading to relatively small sulfur isotope fractionations. Despite this, low seawater sulfate concentration or availability by itself does not adequately explain the anomalous superheavy pyrite values, because microbial culture studies show that sulfur isotope fractionation during BSR approaches zero but does not invert as seawater sulfate declines. Thus, additional mechanism is required.

Abiotic oxidation of dissolved sulfide during sediment reworking has recently been invoked to explain the reversed S isotope fractionation or positive S isotope variations (Aller, 2014; Fike et al., 2015). Experimental studies reveal that abiotic oxidation of dissolved sulfide could result in a fractionation of $\Delta\delta^{34}S_{reactant-product} = \delta^{34}S_{sulfide} - \delta^{34}S_{sulfate} = 5.2 \pm 1.4‰$ (Fry et al., 1988). During abiotic oxidation of sulfide, ^{32}S in sulfide is preferentially oxidized, causing the residual sulfide reservoir to be more enriched in ^{34}S. This mechanism has been proposed to explain the reversed S isotope fractionation in the terminal Ediacaran Nama Group (Ries et al., 2009) and positive $\delta^{34}S_{pyrite}$ values in both modern marine sediments (Gao et al., 2013; Fike et al., 2015) and Triassic strata (Thomazo et al., 2016). However, the limited fractionation (ca. 5‰) associated with abiotic oxidation of sulfide cannot fully explain the large $\delta^{34}S_{pyrite}$ shift in the Khatyspyt Formation. For example, the $\delta^{34}S_{pyrite}$ offset between shallow (as high as 20‰) and deep (as low as −35‰) drill cores of modern marine sediments reaches ca. 55‰ (Fike et al., 2015), which would require almost complete oxidation of sulfide and thus exceedingly low pyrite contents in the sediments. Similarly, the $\delta^{34}S_{pyrite}$ variations in Triassic strata show a large positive excursion from ca. −20‰ to 40‰ (Thomazo et al., 2016), which is also too large to be adequately explained by abiotic oxidation of sulfide.

Bacterial sulfide oxidation may also contribute to the ^{34}S-enrichment of residual sulfide. In experiments with *Thiobacillus concretivorus* grown on H_2S as the sulfur source, enrichment of ^{32}S has been be detected in the product sulfate. Lab results show that sulfur isotope fractionation between initial sulfide and the sulfate product during biological oxidation of H_2S by *Thiobacillus concretivorus* ($\Delta\delta^{34}S_{reactant-product} = \delta^{34}S_{sulfide} - \delta^{34}S_{sulfate}$) can be as much as 9‰ (Kaplan and Rafter, 1958) and up to 18‰ (Kaplan and Rittenberg, 1964). This magnitude of fractionation has not yet been confirmed in natural environment, but its potential role in generating superheavy pyrite should be further investigated in future research.

5.5.2. A synthetic model

In light of increasingly higher TOC content and possible anoxia conditions in the upper Khatyspyt section, it is likely that the large $\delta^{34}S_{pyrite}$ positive shift may reflect enhanced reaction rates of microbial sulfate reduction (MSR) and pyrite formation. Environmentally controlled experiments suggest that MSR-related fractionation is related to sulfate reduction rates that are dependent on the availability of organic substrates as electron donors (Canfield et al., 2010; Leavitt et al., 2013; Wing and Halevy, 2014; Gomes and Hurtgen, 2015), and the degree of S isotope fractionation is inversely proportional to the MSR rate (Harrison and Thode, 1958; Kaplan and Rittenberg, 1964). This mechanism has been well demonstrated in modern marine sediments, particularly in the sulfate–methane transition zone where sufficient methane flux could significantly accelerate the reaction rates of microbial sulfate reduction and cause the production of superhearvy pyrite (Borowski et al., 1996, 2000, 2013; Jørgensen et al., 2004; Q. Lin et al., 2016; Z. Lin et al., 2016).

The occurrences of superheavy pyrite are not limited to the Ediacaran System; in fact, they have also been reported from Tonian-Cryogenian (Xu et al., 1990; Li et al., 1999; Liu et al., 2006; Guilbaud et al., 2015), Cambrian (Gill et al., 2011), and Ordovician strata (Chen et al., 2013; Sim et al., 2015; Kah et al., 2016). However, superheavy pyrite is remarkably common in the Ediacaran System (Canfield, 2001; Prokoph et al., 2008; Canfield and Farquhar, 2012) (Figs. 8 and 9), possibly indicating unusual sulfur cycling and redox conditions in a strongly stratified ocean at the dawn of metazoan diversification (Logan et al., 1995). In the context of a progressively oxidized atmosphere (Shields-Zhou and Och, 2011; Canfield, 2014), enhanced oxidative weathering could have significantly enhanced the continental weathering flux, bring nutrients and sulfate into the terminal Ediacaran ocean, promoting primary production and water column bacterial sulfate reduction (Horton, 2015; Cui et al., 2016a, 2016b). Such a scenario is also consistent with the multiple S isotope study (Wu et al., 2014) and progressive increase in the global seawater $^{87}Sr/^{86}Sr$ ratios during the late Neoproterozoic (Halverson et al., 2007; Shields, 2007; McArthur et al., 2012; Xiao et al., in press). Consistent with this view, largely based on paired S analysis of the time-equivalent Nafun and Ara groups, it was proposed that an increase in pyrite burial, most likely driven by enhanced primary production and sequestration of organic carbon, led

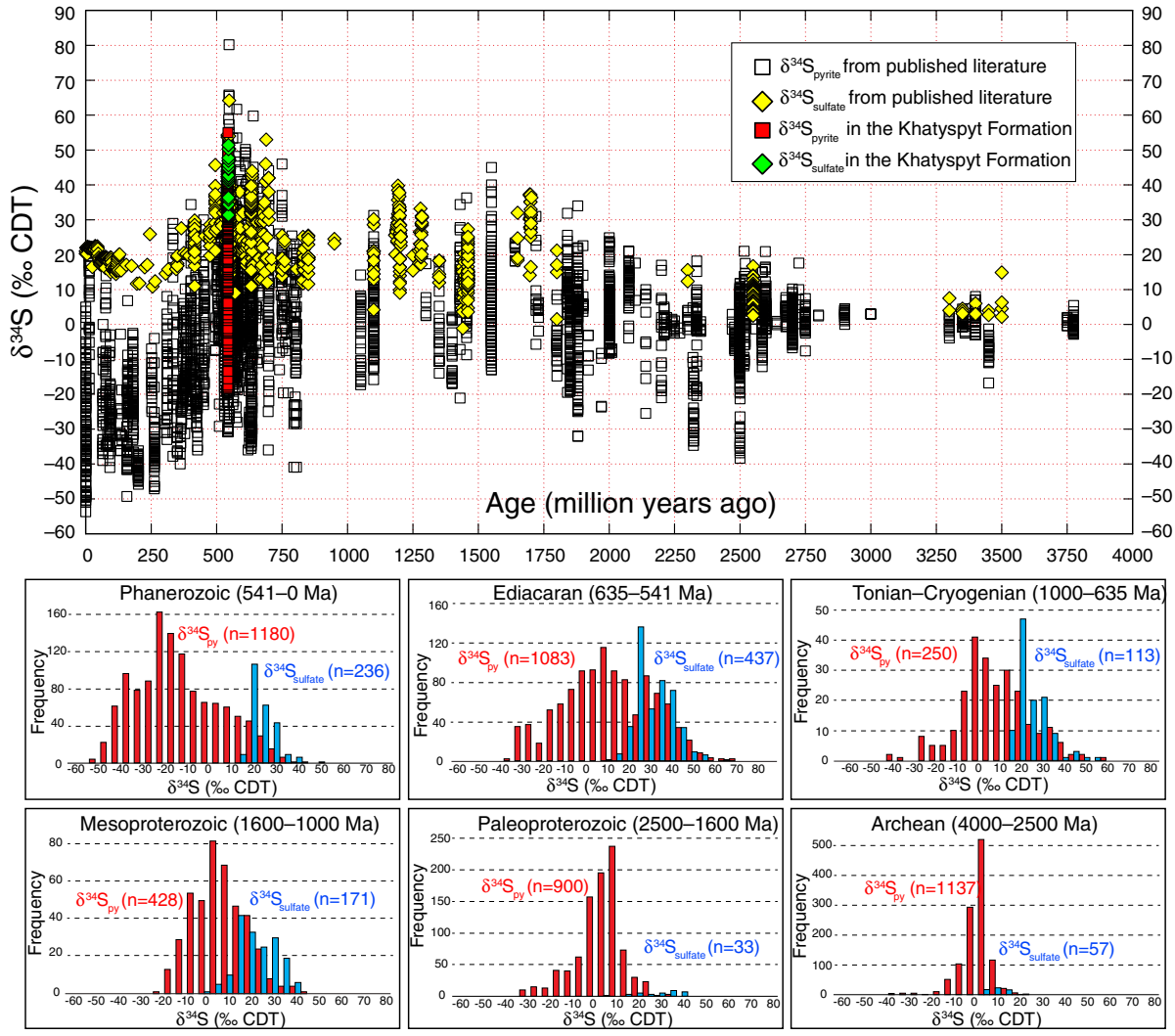

Fig. 9. Evaporite, carbonate-associated sulfate (CAS), and pyrite sulfur isotope data through Earth history. Paired $\delta^{34}S$ data are compiled from the literature [after (Canfield and Farquhar, 2009; Och and Shields-Zhou, 2012; Sahoo et al., 2012; Cui et al., 2016a)]. The small panels are frequency distribution of paired sulfur isotopes of the Phanerozoic (541–0 Ma), Ediacaran (635–541 Ma), Tonian–Cryogenian (1000–635 Ma), Mesoproterozoic (1600–1000 Ma), Paleoproterozoic (2500–1600 Ma), and Archean (4000–2500 Ma). Note the relatively heavier $\delta^{34}S$ data in both sulfate and pyrite during the Ediacaran Period.

to the large paired S isotope anomaly (named Ara anomaly) in the terminal Ediacaran Period (Fike and Grotzinger, 2008), which is notably coupled with earlier reports of elevated oxidation of the atmosphere (Kaufman et al., 2007), enhanced organic carbon burial (Hayes et al., 1999), and widespread phosphorite deposition (Cook and Shergold, 1984; Papineau, 2010; Muscente et al., 2015; Cui et al., 2016b).

5.6. Oceanic redox conditions and fossil distribution

Integrated litho-, bio- and chemo-stratigraphy allows us to uncover possible link between the distribution of early macro-organisms and their paleo-environmental context. The Khatyspyt Formation reveals an intriguing relationship between the first local appearance of Ediacara-type macrofossils and a positive shift in both carbonate carbon and pyrite sulfur isotopes at ca. 42 m in stratigraphy (Fig. 5). The occurrence of Ediacaran fossils in the non-euxunic intervals of the Khatyspyt Formation and the Gaojiashan Member indicates that this overall isotopic-paleontological coupling relationship may reflect a biological response of early macro-organisms to more habitable redox conditions with less hydrogen sulfide in the water column (Fig. 10).

The poisonous nature of dissolved hydrogen sulfide in the water column would have been a source of stress for Ediacaran complex eukaryotes (Anbar and Knoll, 2002), and would have been a major control on where communities would have been able to establish themselves in the Ediacaran oceans (Fig. 10A). As euxinic conditions in the lower Khatyspyt Formation are replaced by non-euxinic and more habitable conditions in the upper Khatyspyt Formation, macrofossils particularly Ediacara-type fossils become more abundant in the upper 85 m of the studied interval (Fig. 10B). Although the atmospheric and oceanic oxygen contents remained below modern levels until the early Paleozoic (Kah and Bartley, 2011; Chen et al., 2015), they may have already crossed the threshold to support animal metabolisms and activities (Knoll and Sperling, 2014; Mills and Canfield, 2014; Mills et al., 2014; Planavsky et al., 2014; Sperling et al., 2015b). Ediacara-type organisms preserved in the Khatyspyt Formation may have lived in non-euxinc (weakly oxic and perhaps ferruginous) conditions. Indeed, iron speciation studies from time-equivalent strata in NW Canada (Johnston et al., 2013; Sperling et al., 2015a) and Namibia (Wood et al., 2015) also support the view that early Ediacaran animals may have lived in dynamic redox environments fluctuating between ferruginous and oxic conditions.

Oceanic euxinia may have been widespread in Mesoproterozoic oceans (Canfield, 1998; Poulton et al., 2004; Scott et al., 2008; Gilleaudeau and Kah, 2013) and may have been common in Ediacaran continental margins due to enhanced oxidative weathering (e.g., Li et al., 2010, 2015a, 2015b; Wang et al., 2012; Och et al., 2015; Sahoo et

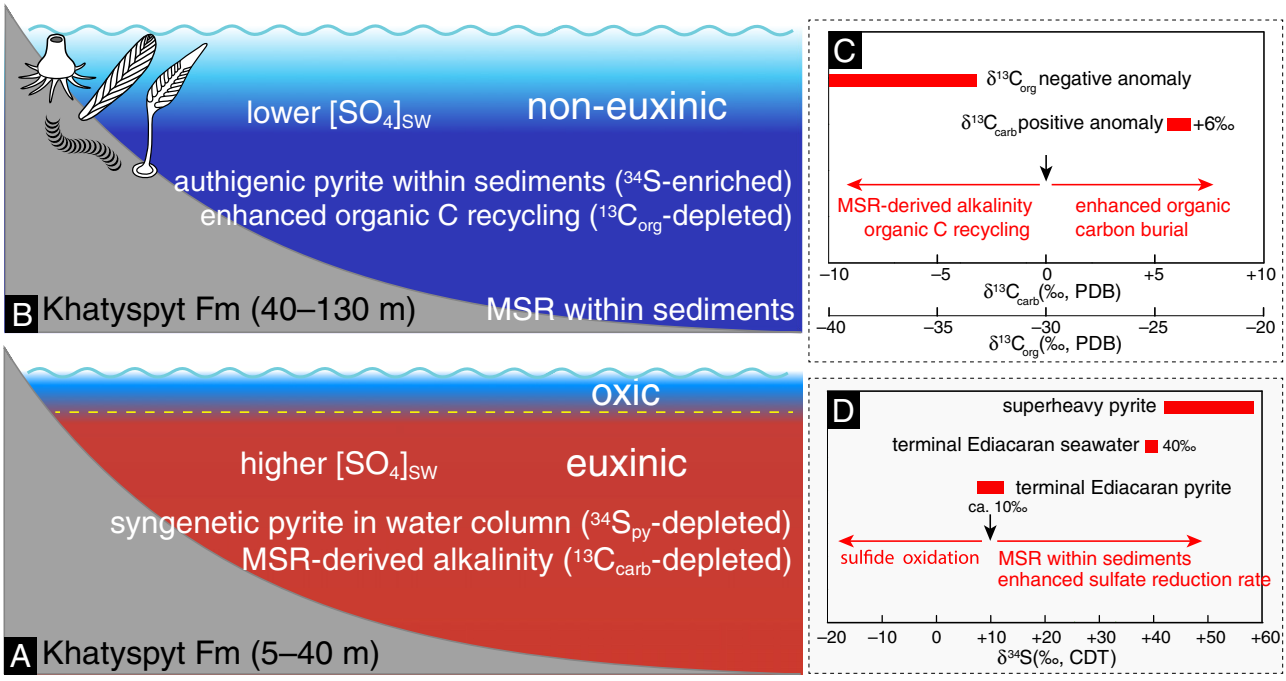

Fig. 10. Biogeochemical model for the Khatyspyt Formation. (A) Redox conditions in the lower studied interval (5–45 m) of the Khatyspyt Formation are characterized by redox stratification with oxic conditions on the surface ocean and euxinic conditions in depth. Microbial sulfate reduction in the euxinic water column leads to more negative $\delta^{13}C_{carb}$ and $\delta^{34}S_{pyrite}$ values. (B) Redox conditions in the upper studied interval (45–130 m) of the Khatyspyt Formation are characterized by non-euxinic conditions with abundant Ediacara-type macrofossils. Ferruginous or oxic conditions drive authigenic pyrite formed within marine sediments, therefore resulting in superheavy pyrite due to limited sulfate concentration in porewaters. (C) Simplified mechanisms for C isotope cycles of the Khatyspyt Formation. MSR = microbial sulfate reduction. (D) Simplified mechanisms for S isotope cycles of the Khatyspyt Formation.

al., 2016). Whether early macro-organisms evolved the capability to detoxify water-column sulfide still remains unknown. Data from this study, however, indicate that the local appearance of Ediacara-type macrofossils in the Khatyspyt Formation does not support the suggestion that early metazoans were capable of tolerating euxinic conditions. If ocean euxinia had a lethal effect on early metazoans, more work is needed to constrain the effect of spatiotemporal variation of euxinic water masses on the distribution of early metazoans (e.g., Li et al., 2010, 2015b; Cui et al., 2015; Och et al., 2015).

6. Conclusions

Based on integrated litho-, bio-, and chemo-stratigraphy of the terminal Ediacaran Khatyspyt Formation in Arctic Siberia, a large positive $\delta^{34}S_{pyrite}$ excursion with a magnitude of ca. 70‰ is reported here for the first time in this time interval. This shift of $\delta^{34}S_{pyrite}$ values from −20‰ to +55‰ is closely coupled with the local appearance of Ediacara-type macrofossils in the studied section, suggesting an intriguing geobiological response of early metazoans to dynamic redox conditions. Based on multiple lines of sedimentological and geochemical evidence, we proposed that euxinic conditions in the continental margin may have excluded Ediacara-type organisms and early metazoans from the lower Khatyspyt Formation. The progressive transition from euxinic to non-euxinic conditions allowed the colonization of early macro-organisms in the upper Khatyspyt Formation.

Acknowledgments

We thank Konstantin Nagovitsin and Boris Kochnev for their assistance in the field; Mike Evans, Rebecca Ohly, Courtney Ray, Rebecca E. Plummer and Yongbo Peng for lab assistance in the UMD Paleoclimate CoLaboratory; and Richard Walker, Igor Puchtel, Jingao Liu and Katherine Bermingham for the guidance on strontium isotope analysis in the UMD TIMS Laboratory. We also thank James Farquhar, Roberta Rudnick, Xianguo Lang, Chuanming Zhou and Jon Husson for helpful discussion in the course of this project. This paper benefits from constructive reviews by Linda Kah and an anonymous reviewer.

This research is funded by the NASA Exobiology grant (NNX12AR91G to AJK and NNX15AL27G to SX), the NSF Sedimentary Geology and Paleontology grant (EAR0844270 to AJK; EAR1528553 to SX), the Carnegie Institution of Washington Postdoctoral Fellowship to XML. Part of the stratigraphic, sedimentological and paleoecological studies of the Khatyspyt Formation was supported by the Russian Science Foundation (grant 14–17–00409 to DVG) and the Committee of the National Geographic Society for Research and Exploration (grants 8227–07, 8637–09, 9031–11 to DVG). HC acknowledges the NASA Astrobiology Institute for support.

Appendix A. Supplementary data

Supplementary data to this article can be found online at http://dx.doi.org/10.1016/j.palaeo.2016.08.015.

References

Aller, R.C., 2014. Sedimentary diagenesis, depositional environments, and benthic fluxes. Treatise Geochem. 8, 293–334.
Amthor, J.E., Grotzinger, J.P., Schröder, S., Bowring, S.A., Ramezani, J., Martin, M.W., Matter, A., 2003. Extinction of *Cloudina* and *Namacalathus* at the Precambrian–Cambrian boundary in Oman. Geology 31, 431–434.
Anbar, A.D., Knoll, A., 2002. Proterozoic ocean chemistry and evolution: a bioinorganic bridge? Science 297, 1137–1142.
Arthur, M.A., 2009. Carbonate rocks deconstructed. Nature 460, 698–699.
Bau, M., Koschinsky, A., Dulski, P., Hein, J.R., 1996. Comparison of the partitioning behaviours of yttrium, rare earth elements, and titanium between hydrogenetic marine ferromanganese crusts and seawater. Geochim. Cosmochim. Acta 60, 1709–1725.
Bengtson, S., Zhao, Y., 1992. Predatorial borings in late Precambrian mineralized exoskeletons. Science 257, 367–369.
Boag, T.H., Darroch, S.A., Laflamme, M., 2016. Ediacaran distributions in space and time: testing assemblage concepts of earliest macroscopic body fossils. Paleobiology http://dx.doi.org/10.1017/pab.2016.20.

Boggiani, P.C., Gaucher, C., Sial, A.N., Babinski, M., Simon, C.M., Riccomini, C., Ferreira, V.P., Fairchild, T.R., 2010. Chemostratigraphy of the Tamengo Formation (Corumbá Group, Brazil): a contribution to the calibration of the Ediacaran carbon-isotope curve. Precambrian Res. 182, 382–401.

Borowski, W.S., Paull, C.K., Ussler, W., 1996. Marine pore-water sulfate profiles indicate in situ methane flux from underlying gas hydrate. Geology 24, 655–658.

Borowski, W.S., Hoehler, T.M., Alperin, M.J., Rodriguez, N.M., Paull, C.K., 2000. Significance of anaerobic methane oxidation in methane-rich sediments overlying the Blake Ridge gas hydrates. Proc. Ocean Drill. Program Sci. Results 87–99.

Borowski, W.S., Rodriguez, N.M., Paull, C.K., Ussler, W., 2013. Are ^{34}S-enriched authigenic sulfide minerals a proxy for elevated methane flux and gas hydrates in the geologic record? Mar. Pet. Geol. 43, 381–395.

Bouougri, E., Porada, H., 2007. Mat-related features from the Terminal Ediacaran Nudaus Formation, Nama Group, Namibia. In: Schieber, J., Bose, P.K., Eriksson, P.G., Banerjee, S., Sarkar, S., Altermann, W., Catuneanu, O. (Eds.), Atlas of Microbial Mat Features Preserved Within the Siliciclastic Rock Record. Elsevier, pp. 214–221.

Bowring, S.A., Grotzinger, J.P., Isachsen, C.E., Knoll, A.H., Pelechaty, S.M., Kolosov, P., 1993. Calibrating rates of Early Cambrian evolution. Science 261, 1293–1298.

Brasier, M.D., McIlroy, D., Liu, A.G., Antcliffe, J.B., Menon, L.R., 2013. The oldest evidence of bioturbation on Earth: comment. Geology 41, e289.

Brocks, J.J., Love, G.D., Summons, R.E., Knoll, A.H., Logan, G.A., Bowden, S.A., 2005. Biomarker evidence for green and purple sulphur bacteria in a stratified Palaeoproterozoic sea. Nature 437, 866–870.

Budd, G.E., Jensen, S., 2015. The origin of the animals and a 'Savannah' hypothesis for early bilaterian evolution. Biol. Rev. http://dx.doi.org/10.1111/brv.12239.

Cai, Y., Hua, H., Xiao, S., Schiffbauer, J.D., Li, P., 2010. Biostratinomy of the late Ediacaran pyritized Gaojiashan Lagerstätte from southern Shaanxi, South China: importance of event deposits. PALAIOS 25, 487–506.

Canfield, D.E., 1998. A new model for Proterozoic ocean chemistry. Nature 396, 450–453.

Canfield, D.E., 2001. Biogeochemistry of sulfur isotopes. In: Valley, J.W., Cole, D. (Eds.), Stable Isotope Geochemistry, Reviews in Mineralogy and Geochemistry. Mineralogical Society of America, pp. 607–636.

Canfield, D.E., 2014. Proterozoic atmospheric oxygen. In: Holland, H.D., Turekian, K.K. (Eds.), Treatise on Geochemistry, 2nd edition Elsevier, Oxford, pp. 197–216.

Canfield, D.E., Farquhar, J., 2009. Animal evolution, bioturbation, and the sulfate concentration of the oceans. Proc. Natl. Acad. Sci. U. S. A. 106, 8123–8127.

Canfield, D.E., Farquhar, J., 2012. The global sulfur cycle. In: Knoll, A.H., Canfield, D.E., Konhauser, K.O. (Eds.), Fundamentals of Geobiology. John Wiley & Sons, Ltd, Oxford, UK, pp. 49–64.

Canfield, D.E., Teske, A., 1996. Late Proterozoic rise in atmospheric oxygen concentration inferred from phylogenetic and sulphur-isotope studies. Nature 382, 127–132.

Canfield, D.E., Poulton, S.W., Narbonne, G.M., 2007. Late-Neoproterozoic deep-ocean oxygenation and the rise of animal life. Science 315, 92–95.

Canfield, D.E., Poulton, S.W., Knoll, A.H., Narbonne, G.M., Ross, G., Goldberg, T., Strauss, H., 2008. Ferruginous conditions dominated later Neoproterozoic deep-water chemistry. Science 321, 949–952.

Canfield, D.E., Farquhar, J., Zerkle, A.L., 2010. High isotope fractionations during sulfate reduction in a low-sulfate euxinic ocean analog. Geology 38, 415–418.

Cao, H., Kaufman, A.J., Shan, X., Cui, H., Zhang, G., 2016. Sulfur isotope constraints on marine transgression in the lacustrine upper cretaceous Songliao Basin, Northeastern China. Palaeogeogr. Palaeoclimatol. Palaeoecol. 451, 152–163.

Chen, D., Wang, J., Racki, G., Li, H., Wang, C., Ma, X., Whalen, M.T., 2013. Large sulphur isotopic perturbations and oceanic changes during the Frasnian–Famennian transition of the Late Devonian. J. Geol. Soc. Lond. 170, 465–476.

Chen, Z., Zhou, C., Xiao, S., Wang, W., Guan, C., Hua, H., Yuan, X., 2014. New Ediacara fossils preserved in marine limestone and their ecological implications. Sci. Rep. 4, 4180.

Chen, X., Ling, H.-F., Vance, D., Shields-Zhou, G.A., Zhu, M., Poulton, S.W., Och, L.M., Jiang, S.-Y., Li, D., Cremonese, L., Archer, C., 2015. Rise to modern levels of ocean oxygenation coincided with the Cambrian radiation of animals. Nat. Commun. 6, 7142.

Clarkson, M., Poulton, S., Guilbaud, R., Wood, R., 2014. Assessing the utility of Fe/Al and Fe-speciation to record water column redox conditions in carbonate-rich sediments. Chem. Geol. 382, 111–122.

Cloud, P.E., 1968. Atmospheric and hydrospheric evolution on the primitive Earth. Science 160, 729–736.

Cloud, P., 1976. Beginnings of biospheric evolution and their biogeochemical consequences. Paleobiology 2, 351–387.

Condon, D., Zhu, M., Bowring, S., Wang, W., Yang, A., Jin, Y., 2005. U–Pb ages from the neoproterozoic Doushantuo Formation, China. Science 308, 95–98.

Cook, P.J., Shergold, J.H., 1984. Phosphorus, phosphorites and skeletal evolution at the Precambrian–Cambrian boundary. Nature 308, 231–236.

Cui, H., 2015. Authigenesis, Biomineralization, and Carbon–Sulfur Cycling in the Ediacaran Ocean Ph.D. dissertation. Department of Geology. University of Maryland, College Park.

Cui, H., Kaufman, A.J., Xiao, S., Zhu, M., Zhou, C., Liu, X.-M., 2015. Redox architecture of an Ediacaran ocean margin: integrated chemostratigraphic (δ^{13}C–δ^{34}S–^{87}Sr/^{86}Sr–Ce/Ce*) correlation of the Doushantuo Formation, South China. Chem. Geol. 405, 48–62.

Cui, H., Alan, K.J., Xiao, S., Zhou, C., 2016. Methane-derived authigenic carbonate linked to the Shuram Excursion: petrographic and geochemical evidence for an early diagenesis origin from the uppermost Doushantuo Formation in South China. Chem. Geol. (under review).

Cui, H., Kaufman, A.J., Xiao, S., Peek, S., Cao, H., Min, X., Cai, Y., Siegel, Z., Liu, X.M., Peng, Y., Schiffbauer, J.D., Martin, A.J., 2016a. Environmental context for the terminal Ediacaran biomineralization of animals. Geobiology 14, 344–363.

Cui, H., Xiao, S., Zhou, C., Peng, Y., Kaufman, A.J., Plummer, R.E., 2016b. Phosphogenesis associated with the Shuram Excursion: petrographic and geochemical observations from the Ediacaran Doushantuo Formation of South China. Sediment. Geol. 341, 134–146.

Darroch, S.A.F., Sperling, E.A., Boag, T.H., Racicot, R.A., Mason, S.J., Morgan, A.S., Tweedt, S., Myrow, P., Johnston, D.T., Erwin, D.H., Laflamme, M., 2015. Biotic replacement and mass extinction of the Ediacara biota. Proc. R. Soc. Lond. B Biol. 282, 20151003.

Darroch, S.A.F., Boag, T.H., Racicot, R.A., Tweedt, S., Mason, S.J., Erwin, D.H., Laflamme, M., 2016. A mixed Ediacaran-metazoan assemblage from the Zaris Sub-basin, Namibia. Palaeogeogr. Palaeoclimatol. Palaeoecol. 459, 198–208.

Derry, L.A., 2010. A burial diagenesis origin for the Ediacaran Shuram–Wonoka carbon isotope anomaly. Earth Planet. Sci. Lett. 294, 152–162.

Derry, L.A., Kaufman, A.J., Jacobsen, S.B., 1992. Sedimentary cycling and environmental change in the Late Proterozoic: evidence from stable and radiogenic isotopes. Geochim. Cosmochim. Acta 56, 1317–1329.

Ding, Q., Chen, Y., 1981. Discovery of soft metazoan from the Sinian system along eastern Yangtze Gorge, Hubei. J. Wuhan Coll. Geol. 2, 53–57 (in Chinese with English abstract).

Duda, J.-P., Blumenberg, M., Thiel, V., Simon, K., Zhu, M., Reitner, J., 2014. Geobiology of a palaeoecosystem with Ediacara-type fossils: the Shibantan Member (Dengying Formation, South China). Precambrian Res. 255, 48–62.

Fedonkin, M.A., 1990. Systematic description of Vendian metazoa. In: Sokolov, B.S., Iwanowski, A.B. (Eds.), The Vendian SystemPaleontology vol. 1. Springer-Verlag, Berlin Heidelberg, Berlin, Germany, pp. 71–120.

Fedonkin, M.A., Gehling, J.G., Grey, K., Narbonne, G.M., Vickers-Rich, P., 2007. The Rise of Animals: Evolution and Diversification of the Kingdom Animalia. John Hopkins University Press, Baltimore, Maryland, USA.

Fike, D.A., Grotzinger, J.P., 2008. A paired sulfate–pyrite δ^{34}S approach to understanding the evolution of the Ediacaran–Cambrian sulfur cycle. Geochim. Cosmochim. Acta 72, 2636–2648.

Fike, D.A., Grotzinger, J.P., 2010. A $\delta^{34}S_{SO4}$ approach to reconstructing biogenic pyrite burial in carbonate–evaporite basins: an example from the Ara Group, Sultanate of Oman. Geology 38, 371–374.

Fike, D.A., Grotzinger, J.P., Pratt, L.M., Summons, R.E., 2006. Oxidation of the Ediacaran ocean. Nature 444, 744–747.

Fike, D.A., Bradley, A.S., Rose, C.V., 2015. Rethinking the ancient sulfur cycle. Annu. Rev. Earth Planet. Sci. 43, 593–622.

Frei, R., Gaucher, C., Døssing, L.N., Sial, A.N., 2011. Chromium isotopes in carbonates — a tracer for climate change and for reconstructing the redox state of ancient seawater. Earth Planet. Sci. Lett. 312, 114–125.

Fry, B., Ruf, W., Gest, H., Hayes, J., 1988. Sulfur isotope effects associated with oxidation of sulfide by O_2 in aqueous solution. Chem. Geol. 73, 205–210.

Gámez Vintaned, J.A., Zhuravlev, A.Y., 2013. The oldest evidence of bioturbation on Earth: comment. Geology 41, e299.

Gao, J., Fike, D.A., Aller, R.C., 2013. Enriched Pyrite δ^{34}S Signals in Modern Tropical Deltaic Muds, 2013 AGU Fall Meeting. American Geophysical Union, San Francisco, p. 0352.

Gaucher, C., Boggiani, P., Sprechmann, P., Sial, A., Fairchild, T., 2003. Integrated correlation of the Vendian to Cambrian Arroyo del Soldado and Corumbá Groups (Uruguay and Brazil): palaeogeographic, palaeoclimatic and palaeobiologic implications. Precambrian Res. 120, 241–278.

Gehling, J.G., 1999. Microbial mats in terminal Proterozoic siliciclastics: Ediacaran death masks. PALAIOS 14, 40–57.

Gehling, J.G., Droser, M.L., 2013. How well do fossil assemblages of the Ediacara biota tell time? Geology 41, 447–450.

Germs, G.J., 1972. New shelly fossils from Nama Group, South West Africa. Am. J. Sci. 272, 752–761.

Gill, B.C., Lyons, T.W., Frank, T.D., 2008. Behavior of carbonate-associated sulfate during meteoric diagenesis and implications for the sulfur isotope paleoproxy. Geochim. Cosmochim. Acta 72, 4699–4711.

Gill, B.C., Lyons, T.W., Young, S.A., Kump, L.R., Knoll, A.H., Saltzman, M.R., 2011. Geochemical evidence for widespread euxinia in the Later Cambrian ocean. Nature 469, 80–83.

Gilleaudeau, G.J., Kah, L.C., 2013. Oceanic molybdenum drawdown by epeiric sea expansion in the Mesoproterozoic. Chem. Geol. 356, 21–37.

Gomes, M.L., Hurtgen, M.T., 2015. Sulfur isotope fractionation in modern euxinic systems: implications for paleoenvironmental reconstructions of paired sulfate–sulfide isotope records. Geochim. Cosmochim. Acta 157, 39–55.

Grazhdankin, D., 2004. Patterns of distribution in the Ediacaran biotas: facies versus biogeography and evolution. Paleobiology 30, 203–221.

Grazhdankin, D.V., 2011. Ediacaran Biota. In: Reitner, J., Thiel, V. (Eds.), Encyclopedia of Geobiology. Springer, Netherlands, pp. 342–348.

Grazhdankin, D.V., 2014. Patterns of evolution of the Ediacaran soft-bodied biota. J. Paleontol. 88, 269–283.

Grazhdankin, D., Gerdes, G., 2007. Ediacaran microbial colonies. Lethaia 40, 201–210.

Grazhdankin, D.V., Balthasar, U., Nagovitsin, K.E., Kochnev, B.B., 2008. Carbonate-hosted Avalon-type fossils in arctic Siberia. Geology 36, 803–806.

Grotzinger, J., Al-Rawahi, Z., 2014. Depositional facies and platform architecture of microbialite-dominated carbonate reservoirs, Ediacaran–Cambrian Ara Group, Sultanate of Oman. AAPG Bull. 98, 1453–1494.

Grotzinger, J.P., Bowring, B.Z., Saylor, B.Z., Kaufman, A.J., 1995. Biostratigraphic and geochronologic constraints on early animal evolution. Science 270, 598–604.

Guilbaud, R., Poulton, S.W., Butterfield, N.J., Zhu, M., Shields-Zhou, G.A., 2015. A global transition to ferruginous conditions in the early Neoproterozoic oceans. Nat. Geosci. 8, 466–470.

Guo, H., Du, Y., Kah, L.C., Hu, C., Huang, J., Huang, H., Yu, W., Song, H., 2015. Sulfur isotope composition of carbonate-associated sulfate from the Mesoproterozoic Jixian Group, North China: implications for the marine sulfur cycle. Precambrian Res. 266, 319–336.

Habicht, K.S., Gade, M., Thamdrup, B., Berg, P., Canfield, D.E., 2002. Calibration of sulfate levels in the Archean ocean. Science 298, 2372–2374.

Hall, M., Kaufman, A.J., Vickers-Rich, P., Ivantsov, A., Trusler, P., Linnemann, U., Hofmann, M., Elliott, D., Cui, H., Fedonkin, M., Hoffmann, K.-H., Wilson, S.A., Schneider, G., Smith, J., 2013. Stratigraphy, palaeontology and geochemistry of the late Neoproterozoic Aar

Member, southwest Namibia: reflecting environmental controls on Ediacara fossil preservation during the terminal Proterozoic in African Gondwana. Precambrian Res. 238, 214–232.
Halverson, G.P., 2006. A Neoproterozoic chronology. In: Xiao, S., Kaufman, A.J. (Eds.), Neoproterozoic Geobiology and Paleobiology. Springer, Berlin, Germany, pp. 231–271.
Halverson, G.P., Dudás, F.Ö., Maloof, A.C., Bowring, S.A., 2007. Evolution of the $^{87}Sr/^{86}Sr$ composition of Neoproterozoic seawater. Palaeogeogr. Palaeoclimatol. Palaeoecol. 256, 103–129.
Harrison, A., Thode, H., 1958. Mechanism of the bacterial reduction of sulfate from isotope fractionation studies. Trans. Faraday Soc. 54, 84–92.
Hayes, J.M., 1993. Factors controlling ^{13}C contents of sedimentary organic compounds: principles and evidence. Mar. Geol. 113, 111–125.
Hayes, J.M., Strauss, H., Kaufman, A.J., 1999. The abundance of ^{13}C in marine organic matter and isotopic fractionation in the global biogeochemical cycle of carbon during the past 800 Ma. Chem. Geol. 161, 103–125.
Hofmann, H., O'brien, S., King, A., 2008. Ediacaran biota on bonavista peninsula, Newfoundland, Canada. J. Paleontol. 82, 1–36.
Horton, F., 2015. Did phosphorus derived from the weathering of large igneous provinces fertilize the Neoproterozoic ocean? Geochem. Geophys. Geosyst. 16, 1723–1738.
Houghton, J., Fike, D., Druschel, G., Orphan, V., Hoehler, T.M., Des Marais, D.J., 2014. Spatial variability in photosynthetic and heterotrophic activity drives localized $\delta^{13}C_{org}$ fluctuations and carbonate precipitation in hypersaline microbial mats. Geobiology 12, 557–574.
Hua, H., Chen, Z., Zhang, L.-y., 2004. *Shaanxilithes* from lower Taozichong Formation, Guizhou Province and its geological and paleobiological significance. J. Stratigr. 28, 265–269 (in Chinese).
Jiang, G., Kaufman, A.J., Christie-Blick, N., Zhang, S., Wu, H., 2007. Carbon isotope variability across the Ediacaran Yangtze platform in South China: implications for a large surface-to-deep ocean $\delta^{13}C$ gradient. Earth Planet. Sci. Lett. 261, 303–320.
Jiang, G., Wang, X., Shi, X., Xiao, S., Zhang, S., Dong, J., 2012. The origin of decoupled carbonate and organic carbon isotope signatures in the early Cambrian (ca. 542–520 Ma) Yangtze platform. Earth Planet. Sci. Lett. 317–318, 96–110.
Johnston, D.T., Wolfe-Simon, F., Pearson, A., Knoll, A.H., 2009. Anoxygenic photosynthesis modulated Proterozoic oxygen and sustained Earth's middle age. Proc. Natl. Acad. Sci. U. S. A. 106, 16925–16929.
Johnston, D.T., Poulton, S.W., Tosca, N.J., O'Brien, T., Halverson, G.P., Schrag, D.P., Macdonald, F.A., 2013. Searching for an oxygenation event in the fossiliferous Ediacaran of northwestern Canada. Chem. Geol. 362, 273–286.
Jørgensen, B.B., Böttcher, M.E., Lüschen, H., Neretin, L.N., Volkov, I.I., 2004. Anaerobic methane oxidation and a deep H_2S sink generate isotopically heavy sulfides in Black Sea sediments 1. Geochim. Cosmochim. Acta 68, 2095–2118.
Kah, L.C., Bartley, J.K., 2011. Protracted oxygenation of the Proterozoic biosphere. Int. Geol. Rev. 53, 1424–1442.
Kah, L.C., Lyons, T.W., Frank, T.D., 2004. Low marine sulphate and protracted oxygenation of the Proterozoic biosphere. Nature 431, 834–838.
Kah, L.C., Thompson, C.K., Henderson, M.A., Zhan, R., 2016. Behavior of marine sulfur in the Ordovician. Palaeogeogr. Palaeoclimatol. Palaeoecol. 458, 133–153.
Kaplan, I.R., Rafter, T.A., 1958. Fractionation of stable isotopes of sulfur by Thiobacilli. Science 127, 517–518.
Kaplan, I.R., Rittenberg, S.C., 1964. Microbiological fractionation of sulphur isotopes. Microbiology 34, 195–212.
Kaufman, A.J., Hayes, J.M., Knoll, A.H., Germs, G.J.B., 1991. Isotopic compositions of carbonates and organic carbon from upper Proterozoic successions in Namibia: stratigraphic variation and the effects of diagenesis and metamorphism. Precambrian Res. 49, 301–327.
Kaufman, A.J., Jacobsen, S.B., Knoll, A.H., 1993. The Vendian record of Sr and C isotopic variations in seawater: implications for tectonics and paleoclimate. Earth Planet. Sci. Lett. 120, 409–430.
Kaufman, A.J., Corsetti, F.A., Varni, M.A., 2007. The effect of rising atmospheric oxygen on carbon and sulfur isotope anomalies in the Neoproterozoic Johnnie Formation, Death Valley, USA. Chem. Geol. 237, 47–63.
Kaufman, A.J., Peek, S., Aaron, J., Cui, H., Grazhdankin, D., Rogov, V., Xiao, S., Buchwaldt, R., Bowring, S., 2012. A Shorter Fuse for the Cambrian Explosion?, 2012 GSA Annual Meeting. The Geological Society of America, Charlotte, North Carolina, USA.
Knauth, L.P., Kennedy, M.J., 2009. The late Precambrian greening of the Earth. Nature 460, 728–732.
Knoll, A.H., Sperling, E.A., 2014. Oxygen and animals in Earth history. Proc. Natl. Acad. Sci. U. S. A. 111, 3907–3908.
Knoll, A.H., Grotzinger, J.P., Kaufman, A.J., Kolosov, P., 1995. Integrated approaches to terminal Proterozoic stratigraphy: an example from the Olenek Uplift, northeastern Siberia. Precambrian Res. 73, 251–270.
Kolesnikov, A.V., Marusin, V.V., Nagovitsin, K.E., Maslov, A.V., Grazhdankin, D.V., 2015. Ediacaran biota in the aftermath of the Kotlinian Crisis: Asha Group of the South Urals. Precambrian Res. 263, 59–78.
Kump, L.R., 2008. The rise of atmospheric oxygen. Nature 451, 277–278.
Lawrence, M.G., Greig, A., Collerson, K.D., Kamber, B.S., 2006. Rare earth element and yttrium variability in South East Queensland waterways. Aquat. Geochem. 12, 39–72.
Leavitt, W.D., Bradley, A.S., Halevy, I., Johnston, D.T., 2013. Influence of sulfate reduction rates on the Phanerozoic sulfur isotope record. Proc. Natl. Acad. Sci. U. S. A. 110, 11244–11249.
Li, R., Chen, J., Zhang, S., Lei, J., Shen, Y., Chen, X., 1999. Spatial and temporal variations in carbon and sulfur isotopic compositions of Sinian sedimentary rocks in the Yangtze platform, South China. Precambrian Res. 97, 59–75.
Li, C., Love, G.D., Lyons, T.W., Fike, D.A., Sessions, A.L., Chu, X., 2010. A stratified redox model for the Ediacaran ocean. Science 328, 80–83.
Li, C., Cheng, M., Algeo, T.J., Xie, S., 2015a. A theoretical prediction of chemical zonation in early oceans (>520 Ma). Sci. China Earth Sci. 11, 1901–1909.
Li, C., Planavsky, N.J., Shi, W., Zhang, Z., Zhou, C., Cheng, M., Tarhan, L.G., Luo, G., Xie, S., 2015b. Ediacaran marine redox heterogeneity and early animal ecosystems. Sci. Rep. 5, 17097.
Lin, Q., Wang, J., Algeo, T.J., Sun, F., Lin, R., 2016a. Enhanced framboidal pyrite formation related to anaerobic oxidation of methane in the sulfate-methane transition zone of the northern South China Sea. Mar. Geol. 379, 100–108.
Lin, Z., Sun, X., Peckmann, J., Lu, Y., Xu, L., Strauss, H., Zhou, H., Gong, J., Lu, H., Teichert, B.M.A., 2016b. How sulfate-driven anaerobic oxidation of methane affects the sulfur isotopic composition of pyrite: a SIMS study from the South China Sea. Chem. Geol. 440, 26–41.
Ling, H.-F., Chen, X., Li, D., Wang, D., Shields-Zhou, G.A., Zhu, M., 2013. Cerium anomaly variations in Ediacaran–earliest Cambrian carbonates from the Yangtze Gorges area, South China: implications for oxygenation of coeval shallow seawater. Precambrian Res. 225, 110–127.
Liu, T.-b., Maynard, J.B., Alten, J., 2006. Superheavy S isotopes from glacier-associated sediments of the Neoproterozoic of south China: oceanic anoxia or sulfate limitation? Geol. Soc. Am. Mem. 198, 205–222.
Liu, X.-M., Kah, L.C., Knoll, A.H., Cui, H., Kaufman, A.J., Shahar, A., Hazen, R.M., 2016. Tracing Earth's O_2 evolution using Zn/Fe ratios in marine carbonates. Geochem. Perspect. Lett. 2, 24–34.
Logan, G.A., Hayes, J., Hieshima, G.B., Summons, R.E., 1995. Terminal Proterozoic reorganization of biogeochemical cycles. Nature 376, 53–56.
Loyd, S.J., Marenco, P.J., Hagadorn, J.W., Lyons, T.W., Kaufman, A.J., Sour-Tovar, F., Corsetti, F.A., 2012. Sustained low marine sulfate concentrations from the Neoproterozoic to the Cambrian: insights from carbonates of northwestern Mexico and eastern California. Earth Planet. Sci. Lett. 339–340, 79–94.
Loyd, S.J., Marenco, P.J., Hagadorn, J.W., Lyons, T.W., Kaufman, A.J., Sour-Tovar, F., Corsetti, F.A., 2013. Local $\delta^{34}S$ variability in ~580 Ma carbonates of northwestern Mexico and the Neoproterozoic marine sulfate reservoir. Precambrian Res. 224, 551–569.
Lyons, T.W., Walter, L.M., Gellatly, A.M., Martini, A.M., Blake, R.E., 2004. Sites of anomalous organic remineralization in the carbonate sediments of South Florida, USA: the sulfur cycle and carbonate-associated sulfate. In: Amend, J.P., Edwards, K.J., Lyons, T.W. (Eds.), Sulfur Biogeochemistry—Past and Present: Geological Society of America Special Paper 379. Geological Society of America, Boulder,Colorado, USA, pp. 161–176.
Lyons, T.W., Reinhard, C.T., Planavsky, N.J., 2014. The rise of oxygen in Earth's early ocean and atmosphere. Nature 506, 307–315.
Macdonald, F.A., Strauss, J.V., Sperling, E.A., Halverson, G.P., Narbonne, G.M., Johnston, D.T., Kunzmann, M., Schrag, D.P., Higgins, J.A., 2013. The stratigraphic relationship between the Shuram carbon isotope excursion, the oxygenation of Neoproterozoic oceans, and the first appearance of the Ediacara biota and bilaterian trace fossils in northwestern Canada. Chem. Geol. 362, 250–272.
Mángano, M.G., Buatois, L.A., 2014. Decoupling of body-plan diversification and ecological structuring during the Ediacaran–Cambrian transition: evolutionary and geobiological feedbacks. Proc. R. Soc. Lond. B Biol. 281, 20140038.
Marenco, P.J., Corsetti, F.A., Hammond, D.E., Kaufman, A.J., Bottjer, D.J., 2008. Oxidation of pyrite during extraction of carbonate associated sulfate. Chem. Geol. 247, 124–132.
McArthur, J.M., Howarth, R.J., Shields, G.A., 2012. Strontium isotope stratigraphy. In: Gradstein, F.M., Ogg, J.G., Schmitz, M.D., Ogg, G.M. (Eds.), The Geologic Time Scale. Elsevier, Boston, pp. 127–144.
McFadden, K.A., Huang, J., Chu, X., Jiang, G., Kaufman, A.J., Zhou, C., Yuan, X., Xiao, S., 2008. Pulsed oxidation and biological evolution in the Ediacaran Doushantuo formation. Proc. Natl. Acad. Sci. U. S. A. 105, 3197–3202.
Meyer, M., Schiffbauer, J.D., Xiao, S., Cai, Y., Hua, H., 2012. Taphonomy of the upper Ediacaran enigmatic ribbonlike fossil *Shaanxilithes*. PALAIOS 27, 354–372.
Mills, D.B., Canfield, D.E., 2014. Oxygen and animal evolution: did a rise of atmospheric oxygen "trigger" the origin of animals? BioEssays 36, 1145–1155.
Mills, D.B., Ward, L.M., Jones, C., Sweeten, B., Forth, M., Treusch, A.H., Canfield, D.E., 2014. Oxygen requirements of the earliest animals. Proc. Natl. Acad. Sci. U. S. A. 111, 4168–4172.
Muscente, A.D., Hawkins, A.D., Xiao, S., 2015. Fossil preservation through phosphatization and silicification in the Ediacaran Doushantuo Formation (South China): a comparative synthesis. Palaeogeogr. Palaeoclimatol. Palaeoecol. 434, 46–62.
Nagovitsin, K.E., Rogov, V.I., Marusin, V.V., Karlova, G.A., Kolesnikov, A.V., Bykova, N.V., Grazhdankin, D.V., 2015. Revised Neoproterozoic and Terreneuvian stratigraphy of the Lena-Anabar Basin and north-western slope of the Olenek Uplift, Siberian Platform. Precambrian Res. 270, 226–245.
Narbonne, G.M., 2005. The Ediacara Biota: Neoproterozoic origin of animals and their ecosystems. Annu. Rev. Earth Planet. Sci. 33, 421–442.
Narbonne, G.M., Kaufman, A.J., Knoll, A.H., 1994. Integrated chemostratigraphy and biostratigraphy of the Windermere Supergroup, northwestern Canada: implications for Neoproterozoic correlations and the early evolution of animals. Geol. Soc. Am. Bull. 106, 1281–1292.
Narbonne, G.M., Laflamme, M., Trusler, P.W., Dalrymple, R.W., Greentree, C., 2014. Deep-water Ediacaran fossils from northwestern Canada: taphonomy, ecology, and evolution. J. Paleontol. 88, 207–223.
Och, L.M., Shields-Zhou, G.A., 2012. The Neoproterozoic oxygenation event: environmental perturbations and biogeochemical cycling. Earth-Sci. Rev. 110, 26–57.
Och, L.M., Cremonese, L., Shields-Zhou, G.A., Poulton, S.W., Struck, U., Ling, H., Li, D., Chen, X., Manning, C., Thirlwall, M., Strauss, H., Zhu, M., 2015. Palaeoceanographic controls on spatial redox distribution over the Yangtze Platform during the Ediacaran–Cambrian transition. Sedimentology 63, 378–410.
Oehlert, A.M., Swart, P.K., 2014. Interpreting carbonate and organic carbon isotope covariance in the sedimentary record. Nat. Commun. 5, 4672.
Oehlert, A.M., Lamb-Wozniak, K.A., Devlin, Q.B., Mackenzie, G.J., Reijmer, J.J.G., Swart, P.K., 2012. The stable carbon isotopic composition of organic material in platform derived sediments: implications for reconstructing the global carbon cycle. Sedimentology 59, 319–335.
Papineau, D., 2010. Global biogeochemical changes at both ends of the Proterozoic: insights from phosphorites. Astrobiology 10, 165–181.

Pelechaty, S.M., Grotzinger, J.P., Kashirtsev, V.A., Zhernovsky, V.P., 1996a. Chemostratigraphic and sequence stratigraphic constraints on Vendian–Cambrian basin dynamics, northeast Siberian craton. J. Geol. 104, 543–563.

Pelechaty, S.M., Kaufman, A.J., Grotzinger, J.P., 1996b. Evaluation of $\delta^{13}C$ chemostratigraphy for intrabasinal correlation: Vendian strata of northeast Siberia. Geol. Soc. Am. Bull. 108, 992–1003.

Peng, Y., Bao, H., Pratt, L.M., Kaufman, A.J., Jiang, G., Boyd, D., Wang, Q., Zhou, C., Yuan, X., Xiao, S., Loyd, S., 2014. Widespread contamination of carbonate-associated sulfate by present-day secondary atmospheric sulfate: evidence from triple oxygen isotopes. Geology 42, 815–818.

Planavsky, N.J., Reinhard, C.T., Wang, X., Thomson, D., McGoldrick, P., Rainbird, R.H., Johnson, T., Fischer, W.W., Lyons, T.W., 2014. Low Mid-Proterozoic atmospheric oxygen levels and the delayed rise of animals. Science 346, 635–638.

Poulton, S.W., Canfield, D.E., 2011. Ferruginous conditions: a dominant feature of the ocean through Earth's history. Elements 7, 107–112.

Poulton, S.W., Fralick, P.W., Canfield, D.E., 2004. The transition to a sulphidic ocean ~1.84 billion years ago. Nature 431, 173–177.

Prokoph, A., Shields, G.A., Veizer, J., 2008. Compilation and time-series analysis of a marine carbonate $\delta^{18}O$, $\delta^{13}C$, $^{87}Sr/^{86}Sr$ and $\delta^{34}S$ database through Earth history. Earth-Sci. Rev. 87, 113–133.

Reinhard, C.T., Planavsky, N.J., Olson, S.L., Lyons, T.W., Erwin, D.H., 2016. Earth's oxygen cycle and the evolution of animal life. Proc. Natl. Acad. Sci. U. S. A. 113, 8933–8938.

Ries, J.B., Fike, D.A., Pratt, L.M., Lyons, T.W., Grotzinger, J.P., 2009. Superheavy pyrite ($\delta^{34}S_{pyr} > \delta^{34}S_{CAS}$) in the terminal Proterozoic Nama Group, southern Namibia: a consequence of low seawater sulfate at the dawn of animal life. Geology 37, 743–746.

Rogov, V.I., Marusin, V., Bykova, N.V., Goy, Y., Nagovitsin, K.E., Kochnev, B.B., Karlova, G., Grazhdankin, D.V., 2012. The oldest evidence of bioturbation on Earth. Geology 40, 395–398.

Rogov, V.I., Marusin, V., Bykova, N., Goy, Y., Nagovitsin, K., Kochnev, B., Karlova, G., Grazhdankin, D.V., 2013a. The oldest evidence of bioturbation on Earth: reply. Geology 41, e290.

Rogov, V.I., Marusin, V., Bykova, N.V., Goy, Y., Nagovitsin, K.E., Kochnev, B.B., Karlova, G., Grazhdankin, D.V., 2013b. The oldest evidence of bioturbation on Earth: reply. Geology 41, e300.

Rogov, V.I., Karlova, G.A., Marusin, V.V., Kochnev, B.B., Nagovitsin, K.E., Grazhdankin, D.V., 2015. Duration of the first biozone in the Siberian hypostratotype of the Vendian. Russ. Geol. Geophys. 56, 573–583.

Sahoo, S.K., Planavsky, N.J., Kendall, B., Wang, X., Shi, X., Scott, C., Anbar, A.D., Lyons, T.W., Jiang, G., 2012. Ocean oxygenation in the wake of the Marinoan glaciation. Nature 489, 546–549.

Sahoo, S.K., Planavsky, N.J., Jiang, G., Kendall, B., Owens, J.D., Wang, X., Shi, X., Anbar, A.D., Lyons, T.W., 2016. Oceanic oxygenation events in the anoxic Ediacaran ocean. Geobiology http://dx.doi.org/10.1111/gbi.12182.

Sansjofre, P., Ader, M., Trindade, R., Elie, M., Lyons, J., Cartigny, P., Nogueira, A., 2011. A carbon isotope challenge to the snowball Earth. Nature 478, 93–96.

Saylor, B.Z., Kaufman, A.J., Grotzinger, J.P., Urban, F., 1998. A composite reference section for terminal Proterozoic strata of southern Namibia. J. Sediment. Res. 68, 1223–1235.

Schiffbauer, J.D., Xiao, S., Cai, Y., Wallace, A.F., Hua, H., Hunter, J., Xu, H., Peng, Y., Kaufman, A.J., 2014. A unifying model for Neoproterozoic–Palaeozoic exceptional fossil preservation through pyritization and carbonaceous compression. Nat. Commun. 5, 5754.

Schobben, M., Stebbins, A., Ghaderi, A., Strauss, H., Korn, D., Korte, C., 2015. Flourishing ocean drives the end-Permian marine mass extinction. Proc. Natl. Acad. Sci. U. S. A. 112, 10298–10303.

Scott, C., Lyons, T.W., Bekker, A., Shen, Y., Poulton, S.W., Chu, X., Anbar, A.D., 2008. Tracing the stepwise oxygenation of the Proterozoic ocean. Nature 452, 456–459.

Shen, B., Xiao, S., Dong, L., Chuanming, Z., Liu, J., 2007. Problematic macrofossils from Ediacaran successions in the North China and Chaidam blocks: implications for their evolutionary roots and biostratigraphic significance. J. Paleontol. 81, 1396–1411.

Shen, B., Xiao, S., Kaufman, A.J., Bao, H., Zhou, C., Wang, H., 2008. Stratification and mixing of a post-glacial Neoproterozoic ocean: evidence from carbon and sulfur isotopes in a cap dolostone from northwest China. Earth Planet. Sci. Lett. 265, 209–228.

Shields, G., 2007. A normalised seawater strontium isotope curve: possible implications for Neoproterozoic–Cambrian weathering rates and the further oxygenation of the Earth. eEarth 2, 35–42.

Shields-Zhou, G., Och, L., 2011. The case for a Neoproterozoic oxygenation event: geochemical evidence and biological consequences. GSA Today 21, 4–11.

Sim, M.S., Ono, S., Hurtgen, M.T., 2015. Sulfur isotope evidence for low and fluctuating sulfate levels in the Late Devonian ocean and the potential link with the mass extinction event. Earth Planet. Sci. Lett. 419, 52–62.

Sokolov, B., Fedonkin, M., 1984. The Vendian as the terminal system of the Precambrian. Episodes 7, 12–19.

Sperling, E.A., Carbone, C., Strauss, J.V., Johnston, D.T., Narbonne, G.M., Macdonald, F.A., 2015a. Oxygen, facies, and secular controls on the appearance of Cryogenian and Ediacaran body and trace fossils in the Mackenzie Mountains of northwestern Canada. Geol. Soc. Am. Bull. 128, 558–575.

Sperling, E.A., Knoll, A.H., Girguis, P.R., 2015b. The ecological physiology of Earth's second oxygen revolution. Annu. Rev. Ecol. Evol. Syst. 46, 215–235.

Sperling, E.A., Wolock, C.J., Morgan, A.S., Gill, B.C., Kunzmann, M., Halverson, G.P., Macdonald, F.A., Knoll, A.H., Johnston, D.T., 2015c. Statistical analysis of iron geochemical data suggests limited late Proterozoic oxygenation. Nature 523, 451–454.

Sun, W., 1986. Late Precambrian pennatulids (sea pens) from the eastern Yangtze Gorge, China: *Paracharnia* gen. nov. Precambrian Res. 31, 361–375.

Tanaka, K., Tani, Y., Takahashi, Y., Tanimizu, M., Suzuki, Y., Kozai, N., Ohnuki, T., 2010. A specific Ce oxidation process during sorption of rare earth elements on biogenic Mn oxide produced by *Acremonium* sp. strain KR21-2. Geochim. Cosmochim. Acta 74, 5463–5477.

Tarhan, L.G., Droser, M.L., 2014. Widespread delayed mixing in early to middle Cambrian marine shelfal settings. Palaeogeogr. Palaeoclimatol. Palaeoecol. 399, 310–322.

Tarhan, L.G., Hughes, N.C., Myrow, P.M., Bhargava, O.N., Ahluwalia, A.D., Kudryavtsev, A.B., 2014. Precambrian–Cambrian boundary interval occurrence and form of the enigmatic tubular body fossil *Shaanxilithes ningqiangensis* from the Lesser Himalaya of India. Palaeontology 57, 283–298.

Tarhan, L.G., Droser, M.L., Planavsky, N.J., Johnston, D.T., 2015. Protracted development of bioturbation through the early Palaeozoic Era. Nat. Geosci. 8, 865–869.

Theiling, B.P., Coleman, M., 2015. Refining the extraction methodology of carbonate associated sulfate: evidence from synthetic and natural carbonate samples. Chem. Geol. 411, 36–48.

Thomazo, C., Vennin, E., Brayard, A., Bour, I., Mathieu, O., Elmeknassi, S., Olivier, N., Escarguel, G., Bylund, K.G., Jenks, J., Stephen, D.A., Fara, E., 2016. A diagenetic control on the Early Triassic Smithian–Spathian carbon isotopic excursions recorded in the marine settings of the Thaynes Group (Utah, USA). Geobiology 14, 220–236.

Thompson, C.K., Kah, L.C., 2012. Sulfur isotope evidence for widespread euxinia and a fluctuating oxycline in Early to Middle Ordovician greenhouse oceans. Palaeogeogr. Palaeoclimatol. Palaeoecol. 313–314, 189–214.

Vishnevskaya, I.A., Kochnev, B.B., Letnikova, E.F., Kiseleva, V.Y., Pisareva, N.I., 2013. Sr isotope signatures in the Vendian Khorbusuonka group of the Olenek uplift (Northeastern Siberian Platform). Dokl. Earth Sci. 449, 298–302.

Wang, L., Shi, X., Jiang, G., 2012. Pyrite morphology and redox fluctuations recorded in the Ediacaran Doushantuo Formation. Palaeogeogr. Palaeoclimatol. Palaeoecol. 333–334, 218–227.

Wang, X., Shi, X., Jiang, G., Tang, D., 2014. Organic carbon isotope gradient and ocean stratification across the late Ediacaran–Early Cambrian Yangtze platform. Sci. China Earth Sci. 57, 919–929.

Warren, L.V., Fairchild, T.R., Gaucher, C., Boggiani, P.C., Poire, D.G., Anelli, L.E., Inchausti, J.C., 2011. *Corumbella* and *in situ Cloudina* in association with thrombolites in the Ediacaran Itapucumi Group, Paraguay. Terra Nova 23, 382–389.

Wing, B.A., Halevy, I., 2014. Intracellular metabolite levels shape sulfur isotope fractionation during microbial sulfate respiration. Proc. Natl. Acad. Sci. U. S. A. 111, 18116–18125.

Wood, R.A., Poulton, S.W., Prave, A.R., Hoffmann, K.H., Clarkson, M.O., Guilbaud, R., Lyne, J.W., Tostevin, R., Bowyer, F., Penny, A.M., Curtis, A., Kasemann, S.A., 2015. Dynamic redox conditions control late Ediacaran metazoan ecosystems in the Nama Group, Namibia. Precambrian Res. 261, 252–271.

Wotte, T., Shields-Zhou, G.A., Strauss, H., 2012. Carbonate-associated sulfate: experimental comparisons of common extraction methods and recommendations toward a standard analytical protocol. Chem. Geol. 326–327, 132–144.

Wu, N., Farquhar, J., Strauss, H., 2014. $\delta^{34}S$ and $\Delta^{33}S$ records of Paleozoic seawater sulfate based on the analysis of carbonate associated sulfate. Earth Planet. Sci. Lett. 399, 44–51.

Wu, C., Zhang, Z., Xiao, J., Fu, Y., Shao, S., Zheng, C., Yao, J., Xiao, C., 2016. Nanhuan manganese deposits within restricted basins of the southeastern Yangtze Platform, China: constraints from geological and geochemical evidence. Ore Geol. Rev. 75, 76–99.

Xiao, S., 2014. Oxygen and early animal evolution. In: Holland, H.D., Turekian, K.K. (Eds.), Treatise on Geochemistry, Second edition The Atmosphere - History vol. 6. Elsevier, Oxford, pp. 231–250.

Xiao, S., Laflamme, M., 2009. On the eve of animal radiation: phylogeny, ecology and evolution of the Ediacara biota. Trends Ecol. Evol. 24, 31–40.

Xiao, S., Yuan, X., Steiner, M., Knoll, A.H., 2002. Macroscopic carbonaceous compressions in a terminal Proterozoic shale: a systematic reassessment of the Miaohe Biota, South China. J. Paleontol. 76, 347–376.

Xiao, S., Shen, B., Zhou, C., Xie, G., Yuan, X., 2005. A uniquely preserved Ediacaran fossil with direct evidence for a quilted bodyplan. Proc. Natl. Acad. Sci. U. S. A. 102, 10227–10232.

Xiao, S., Droser, M., Gehling, J.G., Hughes, I.V., Wan, B., Chen, Z., Yuan, X., 2013. Affirming life aquatic for the Ediacara biota in China and Australia. Geology 41, 1095–1098.

Xiao, S., Narbonne, G.M., Zhou, C., Laflamme, M., Grazhdankin, D.V., Moczydłowska-Vidal, M., Cui, H., 2016. Toward an Ediacaran Time Scale: problems, protocols, and prospects. Episodes (in press).

Xu, X., Huang, H., Liu, B., 1990. Manganese deposits of the Proterozoic Datangpo Formation, South China: genesis and palaeogeography. In: Parnell, J., Ye, L.J., Chen, C.M. (Eds.), Sediment-Hosted Mineral Deposits: Proceedings of a Symposium. Blackwell Publishing Ltd., Oxford, UK, Beijing, People's Republic of China, pp. 39–50 (30 July-4 August 1988).

Zhelezinskaia, I., Kaufman, A.J., Farquhar, J., Cliff, J., 2014. Large sulfur isotope fractionations associated with Neoarchean microbial sulfate reduction. Science 346, 742–744.

Zhou, C., Xiao, S., 2007. Ediacaran $\delta^{13}C$ chemostratigraphy of South China. Chem. Geol. 237, 89–108.

Zhou, C., Jiang, S., Xiao, S., Chen, Z., Yuan, X., 2012. Rare earth elements and carbon isotope geochemistry of the Doushantuo Formation in South China: implication for middle Ediacaran shallow marine redox conditions. Chin. Sci. Bull. 57, 1998–2006.

Zhuravlev, A.Y., Gámez Vintaned, J.A., Ivantsov, A.Y., 2009. First finds of problematic Ediacaran fossil *Gaojiashania* in Siberia and its origin. Geol. Mag. 146, 775–780.